The Influence of Charge States on the π-π Interactions of Aromatic Side Chains with Surface of Graphene Sheet and Single-Walled Carbon-Nanotubes in Bioelectrodes

Dong Xiao, Weichao Sun, Hongjing Dai, Yanfang Zhang, Xin Qin, Li Li, Zidong Wei and Xiaohua Chen*

School of Chemistry and Chemical Engineering, Chongqing University, Chongqing, 400030, China

1. Complete Reference of 42

(41) Frisch, M. J.; Trucks, G. W.; Schlegel, H. B.; Scuseria, G. E.; Robb, M. A.; Cheeseman, J. R.; Scalmani, G.; Barone, V.; Mennucci, B.; Petersson, G. A.; Nakatsuji, H.; Caricato, M.; Li, X.; Hratchian, H. P.; Izmaylov, A. F.; Bloino, J.; Zheng, G.; Sonnenberg, J. L.; Hada, M.; Ehara, M.; Toyota, K.; Fukuda, R.; Hasegawa, J.; Ishida, M.; Nakajima, T.; Honda, Y.; Kitao, O.; Nakai, H.; Vreven, T.; Montgomery, Jr., J. A.; Peralta, J. E.; Ogliaro, F.; Bearpark, M.; Heyd, J. J.; Brothers, E.; Kudin, K. N.; Staroverov, V. N.; Kobayashi, R.; Normand, J.; Raghavachari, K.; Rendell, A.; Burant, J. C.; Iyengar, S. S.; Tomasi, J.; Cossi, M.; Rega, N.; Millam, N. J.; Klene, M.; Knox, J. E.; Cross, J. B.; Bakken, V.; Adamo, C.; Jaramillo, J.; Gomperts, R.; Stratmann, R. E.; Yazyev, O.; Austin, A. J.; Cammi, R.; Pomelli, C.; Ochterski, J. W.; Martin, R. L.; Morokuma, K.; Zakrzewski, V. G.; Voth, G. A.; Salvador, P.; Dannenberg, J. J.; Dapprich, S.; Daniels, A. D.; Farkas, Ö.; Foresman, J. B.; Ortiz, J. V.; Cioslowski, J.; Fox, D. J., *Gaussian 09, Revision D.01;* Gaussian, Inc., Wallingford CT, **2013**.

* *The corresponding authors: Xiaohua Chen, chxh7@cqu.edu.cn*

2. Methods Selecting

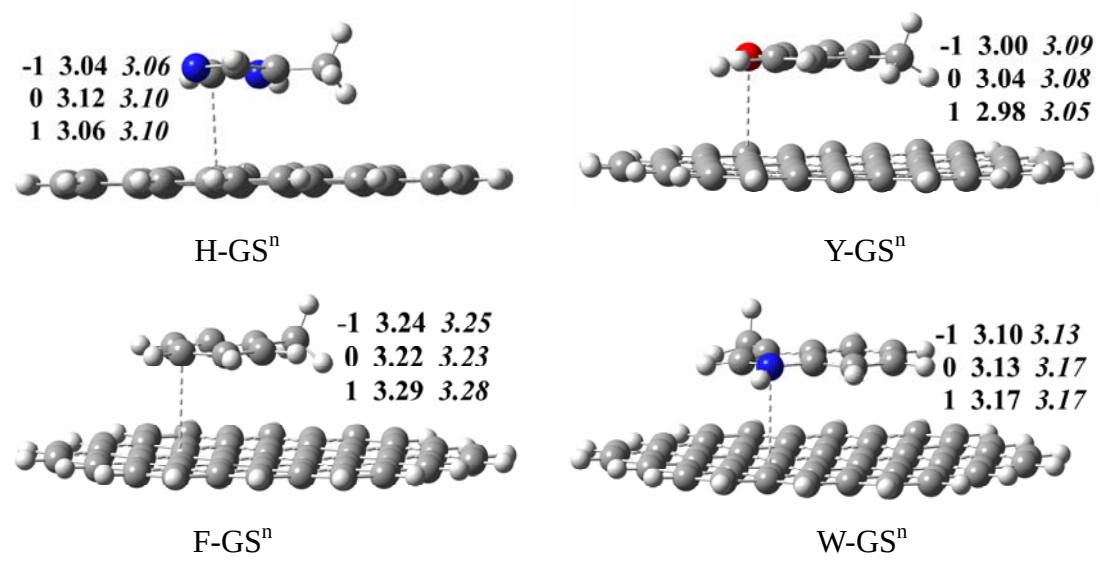

Figure S1. The comparison of the shortest distances between the graphene and aromatic rings for A-GS^n (n= -1, 0, 1) obtain at the M06-2X/6-31G(d) (bold) and M06-2X/6-31+G(d) (italics) levels.

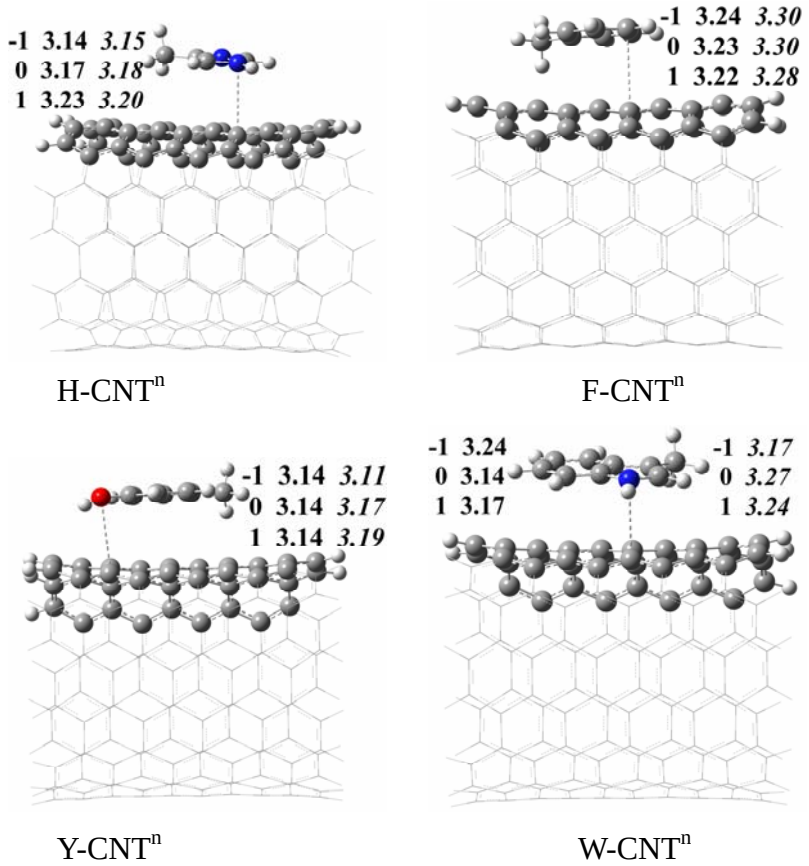

Figure S2. The shortest distances between the CNT and aromatic rings for A-CNT^n (n= 1-, 0, 1) obtain at the M06-2X/6-31G(d) (bold) and ONIOM(M06-2X/6-31+G(d):M06-2X/STO-3G) (italics) levels.

Note: It is clear that the shortest distances obtained by the M06-2X/6-31G(d) calculations are in good agreement with the results of the M06-2X/6-31+G(d) and ONIOM(M06-2X/6-31+G(d):M06-2X/STO-3G) calculations. The agreements reveals that M06-2X shows essentially no dependence on a change in the size and flexibility of the basis set for all the aromatic ring-GS/CNT complexes considered here. To improve the computation efficiency, the M06-2X/6-31+G(d,p)//M06-2X/6-31G(d) method is mainly used to deal with the A-GS^n and A-CNT^n (n= 3-, 2-, 1-, 0, 1, 2, 3) systems in this paper.

Table S1. The Shortest Distances between Methylbenzene and Graphene for F-GS^n (n= 3-, 2-, 1-, 0, 1, 2, 3) Obtains at the M06-2X/6-31G(d), ωB97XD/6-31G(d) and B3P86/6-31G(d) Levels.

F-GS^n	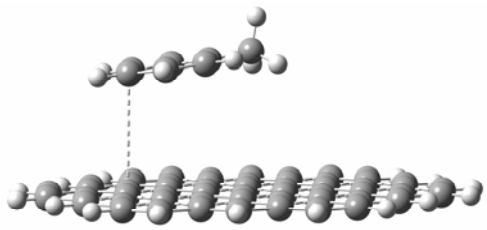						
Charge	-3	-2	-1	0	1	2	3
M06-2X	3.16	3.17	3.24	3.22	3.29	3.28	3.25
ωB97XD	3.24	3.25	3.29	3.27	3.27	3.28	3.27
B3P86	3.60	3.74	3.75	3.70	3.65	3.66	3.92

Notes: The structures of F-GS^n (n=3-, 2-, 1-, 0, 1, 2, 3) are also optimized by the methods of ωD97X and B3P86 with the same basis set of 6-31G(d). It should be noted that the short distances are in the range of 3.24~3.29 Å obtained by the ωD97X/6-31G(d) optimizations, in line with the distances of the M06-2X/6-31G(d) method (3.16~3.29 Å). However, the shortest distances for F-GS^n (n=3-, 2-, 1-, 0, 1, 2, 3) obtained by the B3P86 function is in the range of 3.60~3.92 Å, which are larger than the distances of M06-2X and ωD97X functions. This is because that the B3P86 function can not include the long-range dispersive forces.

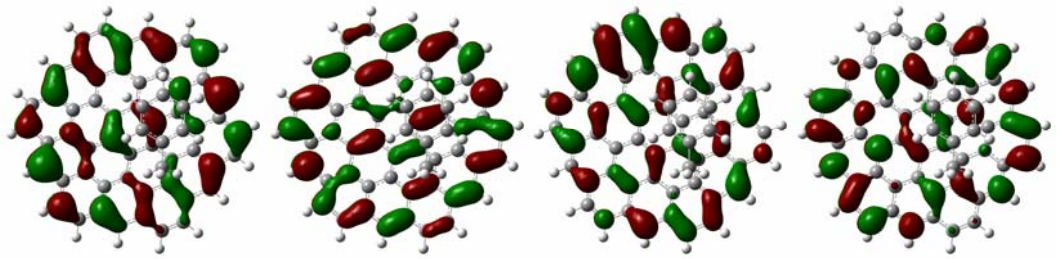

F-GS^{3-} HOMO-1 HOMO SOMO LUMO

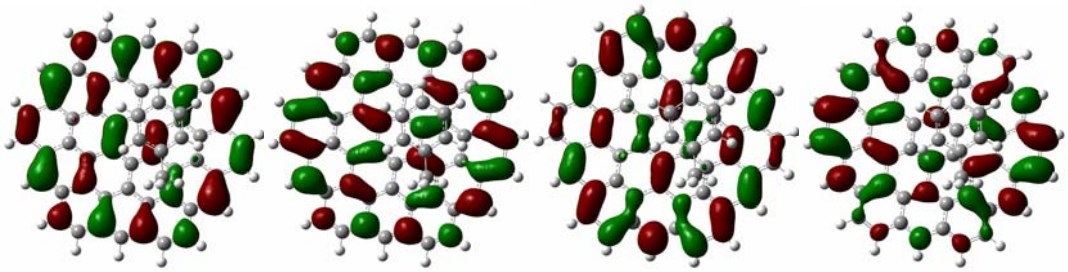

F-GS^{2-} HOMO-1 HOMO LUMO LUMO+1

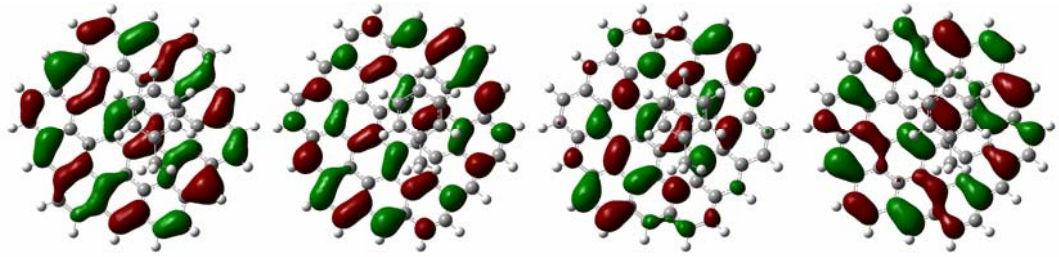

F-GS^{-} HOMO-1 HOMO SOMO LUMO

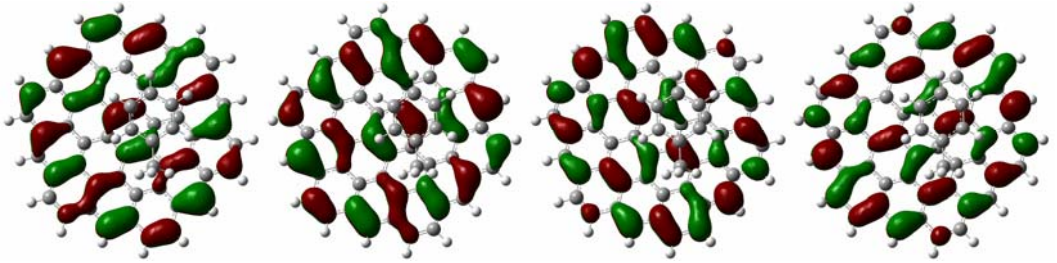

F-GS^{0} HOMO-1 HOMO LUMO LUMO+1

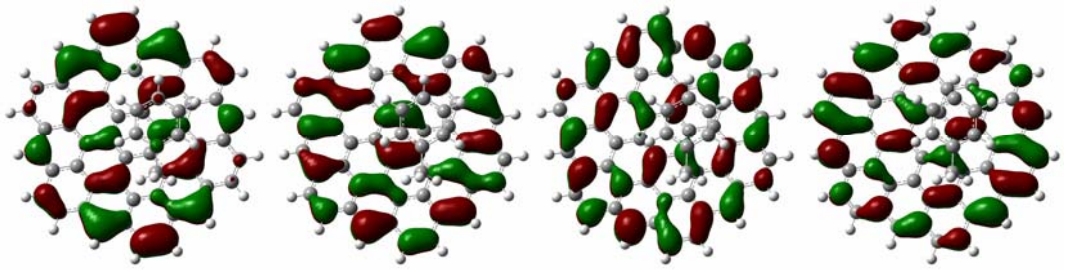

F-GS^{1} HOMO SOMO LUMO LUMO+1

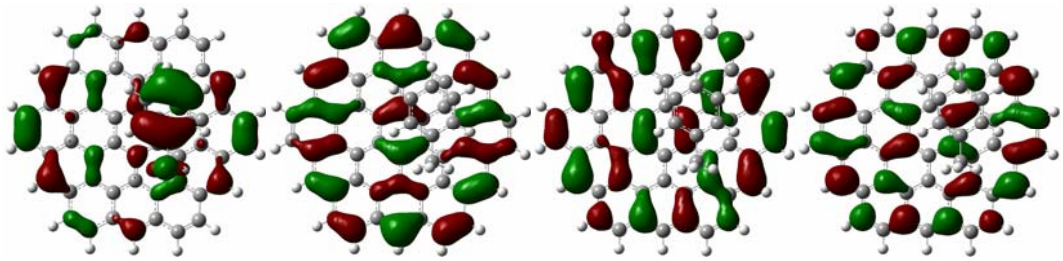

$F\text{-}GS^2$ HOMO-1 HOMO LUMO LUMO+1

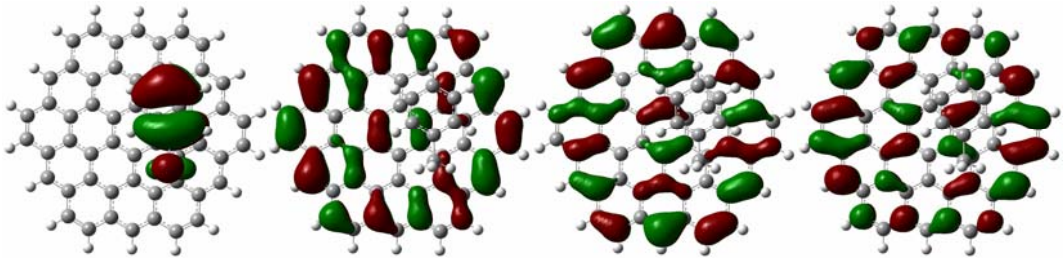

$F\text{-}GS^3$ HOMO SOMO LUMO LUMO+1

Figure S3. The distributions of the front molecular orbitals for the charged F-GS systems obtained at the ωB97XD/6-31G(d) level. Besides, the similar distributions of the front molecular orbitals are found by the B3P86/6-31G(d) and M06-2X/6-31G(d) (Figure S5, below) calculations.

3. Tables and Relations

Table S2. The Distributions of Mulliken Charges for all the A-GS^n and A-CNT^n Systems Obtained at the M06-2X/6-31+G(d,p)//M06-2X/6-31G(d) Level.

Systems	Moiety	-3	-2	-1	0	1	2	3
A-GS^n	H	-0.036	-0.026	-0.094	-0.080	-0.054	0.062	0.126
	GS	-2.964	-1.974	-0.906	0.080	1.054	1.938	2.874
	F	-0.029	0.002	0.020	0.046	0.071	0.152	0.200
	GS	-2.971	-2.002	-1.020	-0.046	0.929	1.848	2.800
	Y	-0.052	-0.010	0.022	0.060	0.063	0.141	**0.679**
	GS	-2.948	-1.990	-1.022	-0.060	0.937	1.859	**2.321**
	W	-0.150	-0.115	-0.085	-0.059	0.042	0.220	**0.799**
	GS	-2.850	-1.885	-0.915	0.059	0.958	1.780	**2.201**
A-CNT^n	H	-0.011	0.014	0.015	0.023	0.028	0.056	0.059
	CNT	-2.989	-2.014	-1.015	-0.023	0.972	1.944	2.941
	F	0.082	0.096	0.111	0.127	0.153	0.176	0.197
	CNT	-3.082	-2.096	-1.111	-0.127	0.847	1.824	2.803
	Y	0.172	0.190	0.200	0.208	0.211	0.195	0.195
	CNT	-3.172	-2.190	-1.200	-0.208	0.789	1.805	2.805
	W	0.042	0.058	0.065	0.114	0.098	0.168	**0.641**
	CNT	-3.042	-2.058	-1.065	-0.114	0.902	1.832	**2.359**

Table S3. The First Adiabatic Electron Affinities (EA_1), the Second Adiabatic Electron Affinities (EA_2), the Third Adiabatic Electron Affinities (EA_3), the First Adiabatic Ionization Energies (IE_1), the Second Adiabatic Ionization Energies (IE_2) and the Third Adiabatic Ionization Energies (IE_3) for all the GS, CNT, A-GS and A-CNT Systems.

(eV)	A-GS				A-CNT				H	F	Y	W	GS	CNT
	H	F	Y	W	H	F	Y	W						
EA_3	3.52	3.70	3.64	3.65	1.95	2.00	1.94	1.98					3.79	1.63
EA_2	1.05	1.18	1.09	1.17	-0.29	-0.25	-0.29	-0.25	2.25	1.36	1.26	1.10	1.21	0.15
EA_1	-1.48	-1.42	-1.48	-1.46	-2.18	-2.14	-2.18	-2.12	8.39	8.79	8.09	7.47	-1.38	-2.15
IE_1	6.56	6.55	6.53	6.55	5.97	5.95	5.96	5.95					6.61	5.98
IE_2	9.23	9.22	9.22	9.13	8.20	7.87	7.87	7.83					9.28	7.91
IE_3	11.78	11.87	11.68	11.52	9.80	10.15	10.12	10.10					11.95	10.21

Note: The values of the adiabatic electron affinities and the adiabatic ionization energies also confirm that the donating and accepting of electrons for the interacted systems of A-GS and A-CNT are only the substrates of the graphene sheet and the CNT.

Table S4. The Binding Energies (in kcal/mol) for the Interactions of Four Aromatic Side Chains with Different Charged GS/CNT at the M06-2X/6-31+G(d,p)//M06-2X/6-31G(d) Level of Theory with the Counterpoise Corrections for the Basis Set Superposition Error (BSSE) Corrections.

GS	-3	-2	-1	0	1	2	3
H	22.2	16.0	12.3	11.2	10.3	12.2	15.9
F	13.8	12.4	11.2	10.8	11.0	12.2	13.9
Y	21.8	18.4	14.5	12.8	12.7	14.9	24.9
W	22.8	18.9	17.3	16.3	16.3	20.8	32.9
(7,7)CNT	-3	-2	-1	0	1	2	3
H	11.6	9.3	8.1	7.4	7.8	8.9	10.8
F	9.5	8.9	8.4	8.5	9.1	9.9	11.1
Y	15.5	12.9	11.2	10.0	10.0	10.8	13.1
W	13.3	11.6	11.0	11.5	12.0	13.8	18.1

Table S5. The Binding Energies (in kcal/mol) for the Interactions of Four Aromatic Side Chains with Different Charged GS/CNT at the M06-2X/6-31+G(d,p)//M06-2X/6-31G(d) Level of Theory without Considering the Counterpoise Corrections for the Basis Set Superposition Error (BSSE).

GS	-3	-2	-1	0	1	2	3
H	24.0	17.4	14.4	13.3	12.5	14.3	18.0
F	15.7	14.2	13.1	12.7	12.9	14.2	15.9
Y	24.4	20.9	17.0	15.4	15.3	17.6	27.5
W	25.6	21.7	20.1	19.1	19.3	23.8	36.1
(7,7)CNT	-3	-2	-1	0	1	2	3
H	13.4	11.4	10.0	9.3	9.7	10.7	12.5
F	11.2	10.4	10.1	10.3	10.9	11.8	13.0
Y	17.8	15.4	13.6	12.6	12.5	13.4	15.7
W	15.8	14.2	13.5	13.9	14.4	16.4	20.8

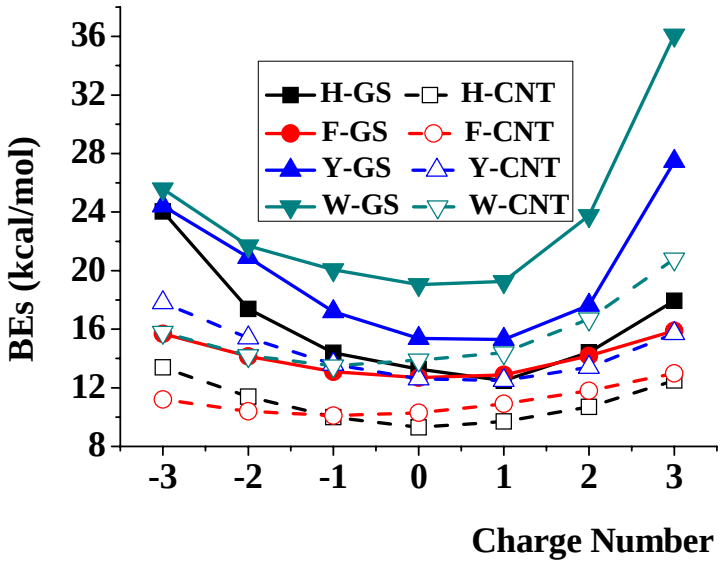

Figure S4. The trend of the binding energies (Table S5) for the interactions of aromatic rings with graphene sheet and (7,7)CNT changes with the different charged states at the M06-2X/6-31+G(d,p)//M06-2X/6-31G(d) level without considering the BSSE corrections.

Table S6. The Binding Energies (BEs, in kcal/mol) for the Interactions of the Four Aromatic Side Chains with Graphene Sheet (GS) and (7,7)-Single-Walled Carbon Nanotube (CNT) at the Charged States of -1, 0 and 1 Obtained at the M06-2X/6-31+G(d) and ONIOM(M06-2X/6-31+G(d):M06-2X/STO-3G) Levels.

BEs(kcal/mol)	Method	Charge	H	F	Y	W
A-GS	M06-2X/6-31+G*	-1	11.1	11.4	14.6	16.4
		0	10.2	10.7	12.6	15.4
		1	10.2	10.7	12.6	15.4
A-CNT	ONIOM(M06-2X/6-31+G(d):M06-2X/STO-3G	-1	10.2	10.6	14.1	13.9
		0	9.3	10.0	12.4	13.6
		1	9.7	10.5	12.5	14.0

Table S7. The Distributions of Mulliken Charges for all the A-CNT^n Systems (n = -1, 0, 1) Obtained at the ONIOM(M06-2X/6-31+G(d):M06-2X/STO-3G Level.

Systems	Moiety	-1	0	1
H-CNT^n	H	-0.0045	-0.0030	0.0010
	High	-0.2936	-0.0184	0.2607
	Low	-0.7019	0.0214	0.7383
F-CNT^n	F	-0.0025	0.0005	0.0020
	High	-0.2446	-0.0045	0.2559
	Low	-0.7528	0.0039	0.7421
Y-CNT^n	Y	0.0006	0.0017	0.0064
	High	-0.2524	0.0109	0.2828
	Low	-0.7482	-0.0125	0.7108
W-CNT^n	W	-0.0163	-0.0016	0.0040
	High	-0.2800	-0.0126	0.2474
	Low	-0.7037	0.0142	0.7486

Table S8. The Distributions of Natural Charges for all the A-GS^n Systems Obtained through the Natural Bond Orbital (NBO) Calculations at the M06-2X/6-31+G(d,p)//M06-2X/6-31G(d) Level.

Systems	Moiety	-3	-2	-1	0	1	2	3
A-GS^n	H	-0.012	-0.007	0.002	0.006	0.015	0.068	0.141
	GS	-2.971	-1.993	-1.002	-0.006	0.985	1.932	2.860
	F	-0.022	-0.016	-0.008	-0.004	0.002	0.016	0.034
	GS	-2.971	-1.984	-0.992	0.004	0.998	2.048	2.966
	Y	-0.018	-0.010	-0.020	0.003	0.012	0.034	0.629
	GS	-2.982	-1.989	-1.171	-0.003	0.988	1.966	2.371
	W	-0.013	-0.009	0.000	0.007	0.060	0.229	0.880
	GS	-2.987	-1.991	-1.000	-0.007	0.940	1.814	2.120

Note: A comparison between the data in Table S8 and the data in Table S2 reveals that the Mulliken charge distributions between the graphene and aromatic rings are nearly consistent with the NBO charge distributions. In addition, we mainly examined the changing tend of charge distributions with the varying charge states in this paper. Therefore, the Mulliken atomic charges are used in the main text.

4. Front Molecular Orbitals

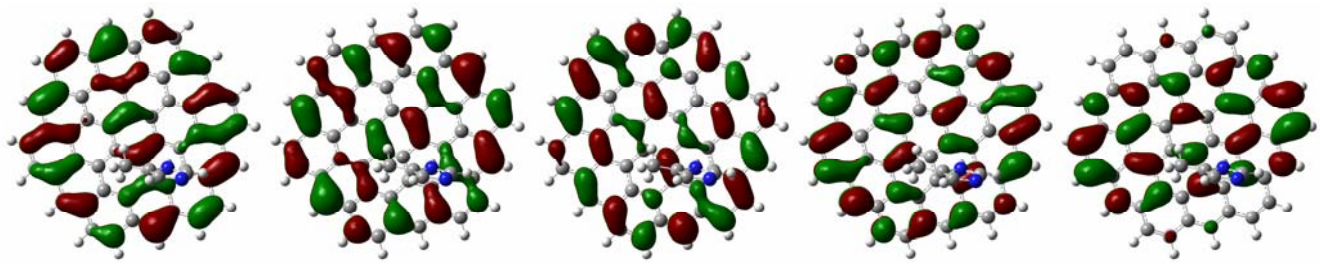

H-GS^{3-} HDMO-2 HDMO-1 HDMO SOMO LUMO+1

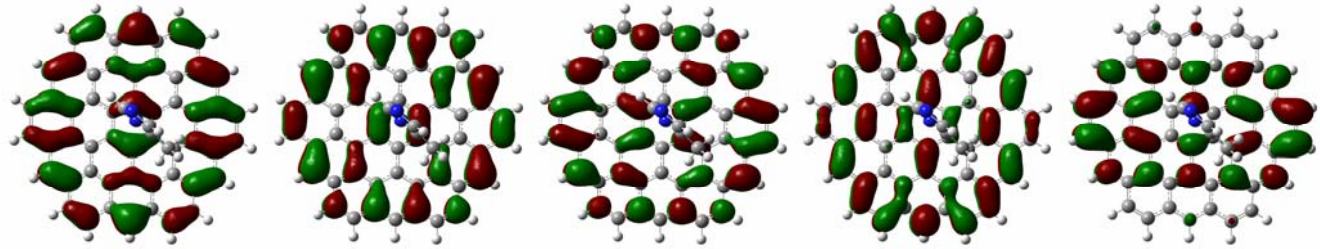

H-GS^{2-} HDMO-2 HDMO-1 HDMO LUMO LUMO+1

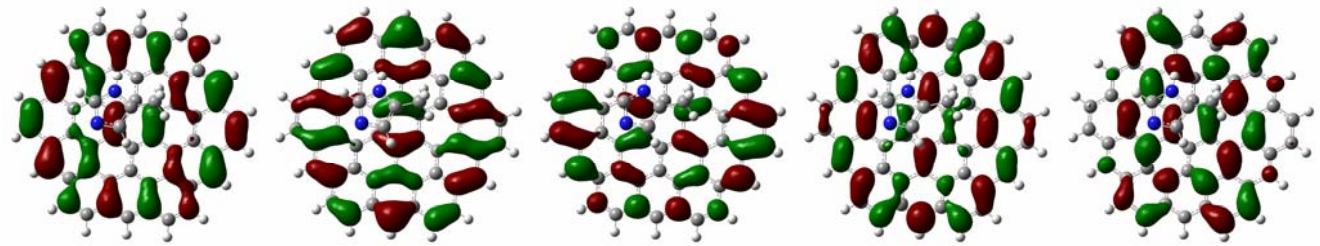

H-GS^{-} HDMO-1 HDMO SOMO LUMO LUMO+1

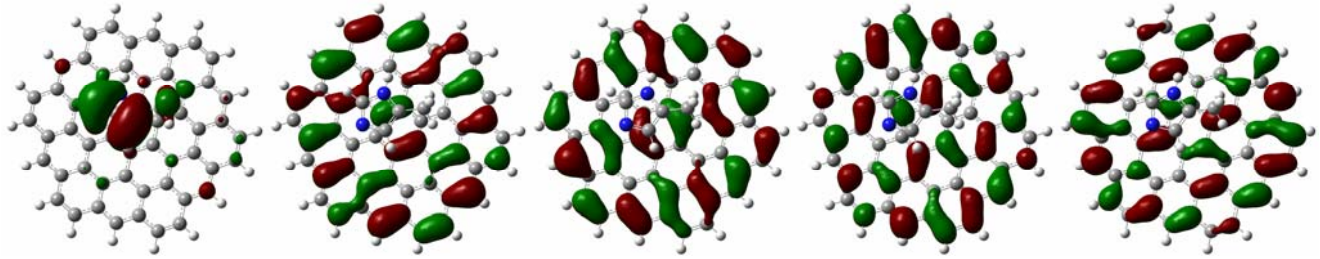

H-GS^{0} HDMO-2 HDMO-1 HDMO LUMO LUMO+1

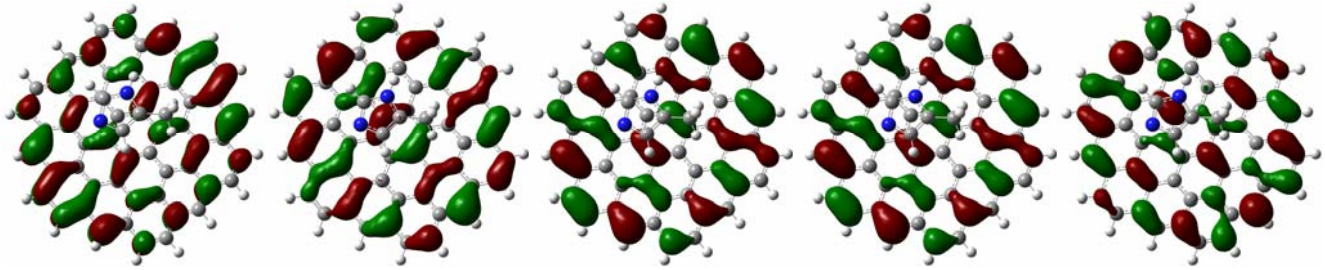

H-GS^{+} HDMO-1 HDMO SOMO LUMO LUMO+1

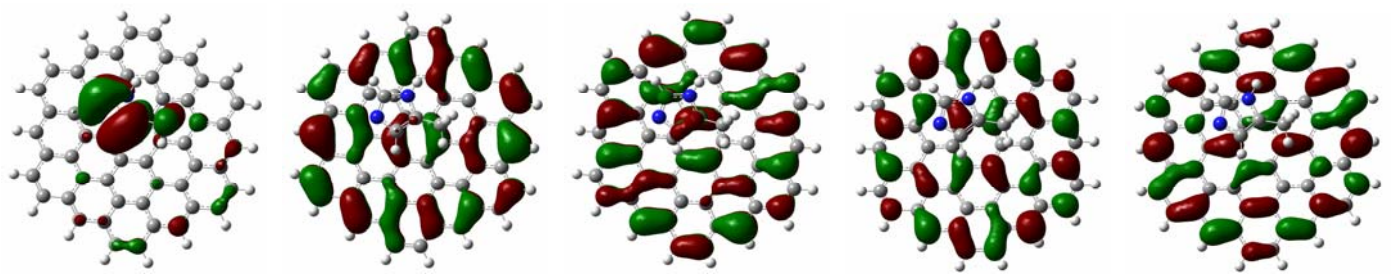

H-GS^{2+} HDMO-1 HDMO LUMO LUMO+1 LUMO+2

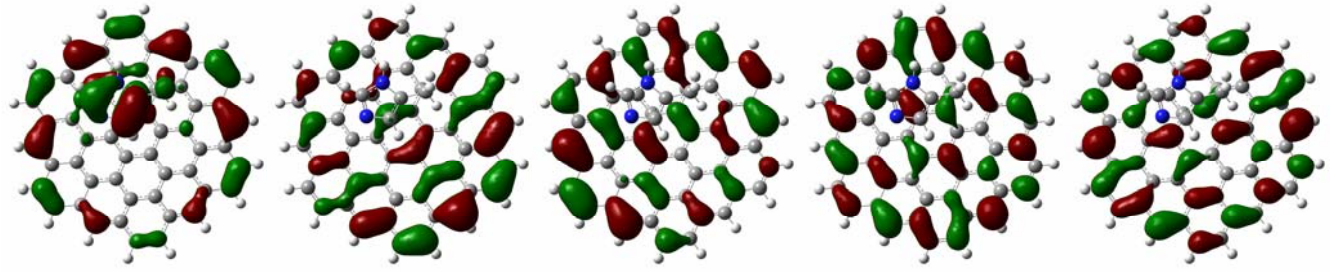

H-GS^{3+} HDMO SOMO LUMO LUMO+1 LUMO+2

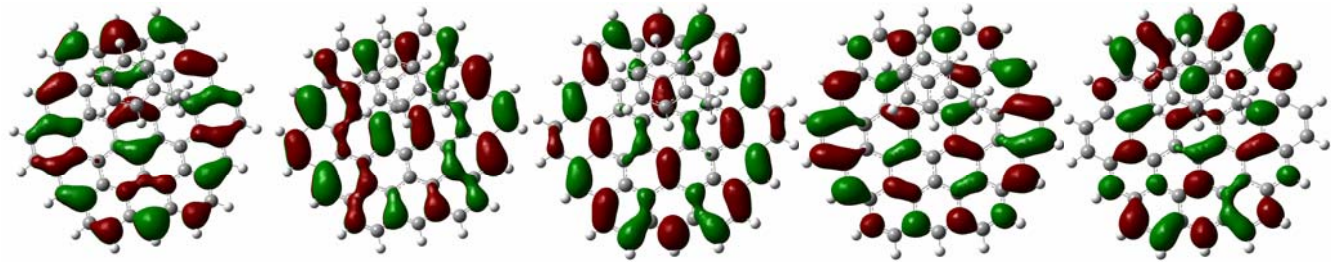

F-GS^{3-} HDMO-2 HDMO-1 HDMO SOMO LUMO

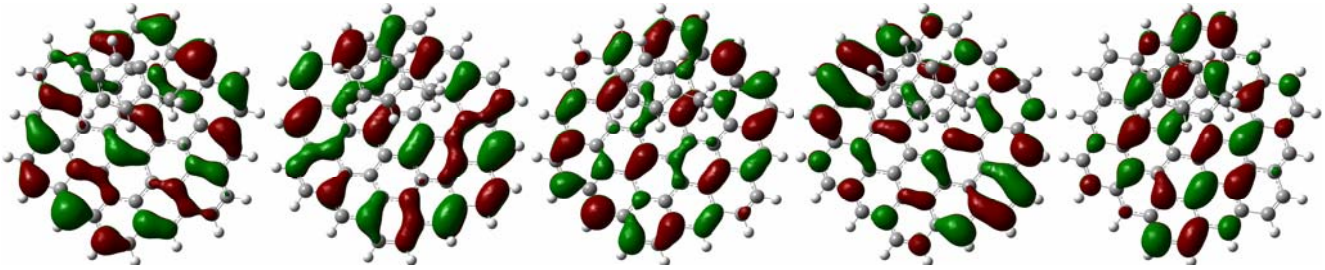

F-GS^{2-} HDMO-2 HDMO-1 HDMO LUMO LUMO+1

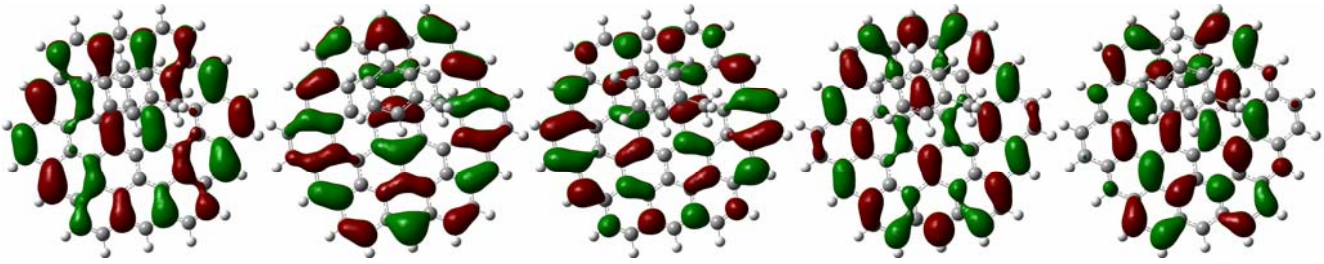

F-GS^{-} HDMO-1 HDMO SOMO LUMO LUMO+1

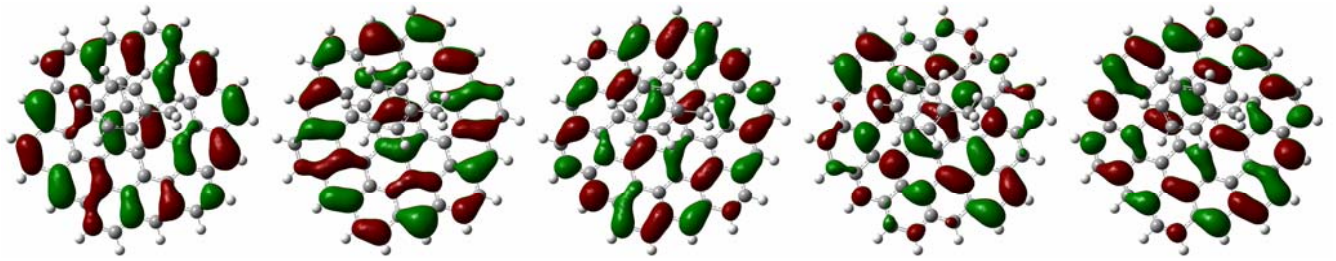

F-GS^{0} HDMO-2 HDMO-1 HDMO LUMO LUMO+1

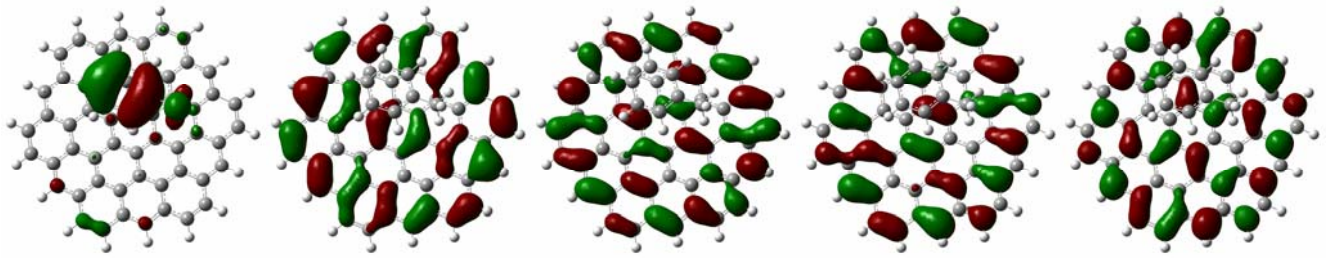

F-GS^{+} HDMO-1 HDMO SOMO LUMO LUMO+1

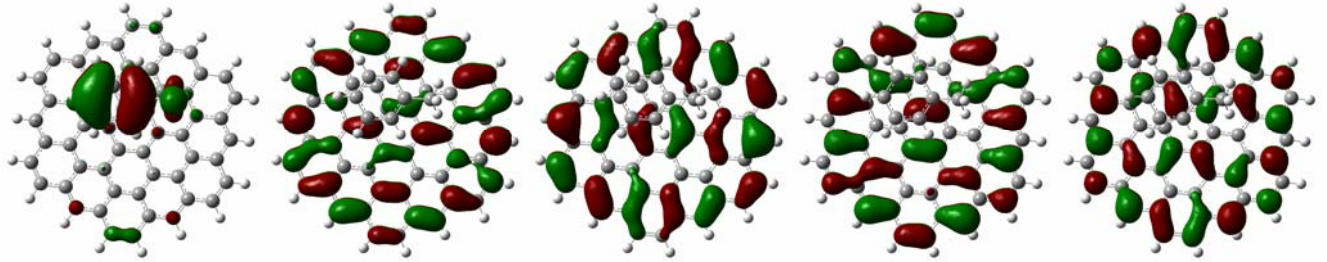

F-GS^{2+} HDMO-1 HDMO LUMO LUMO+1 LUMO+2

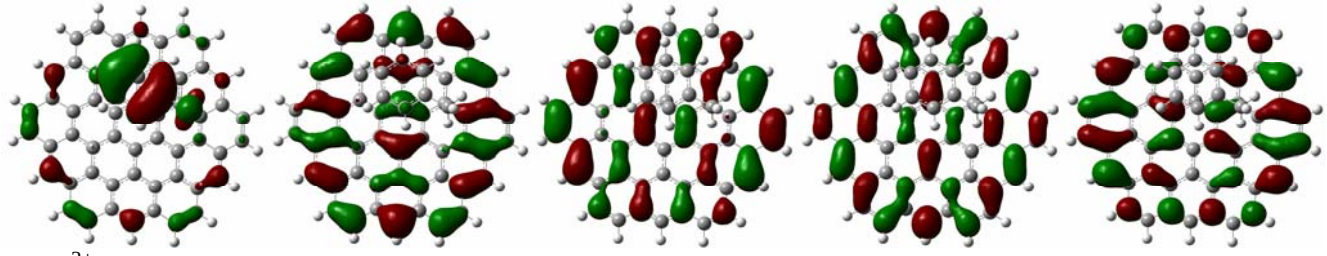

F-GS^{3+} HDMO SOMO LUMO LUMO+1 LUMO+2

Y-GS^{3-} HDMO-2 HDMO-1 HDMO SOMO LUMO

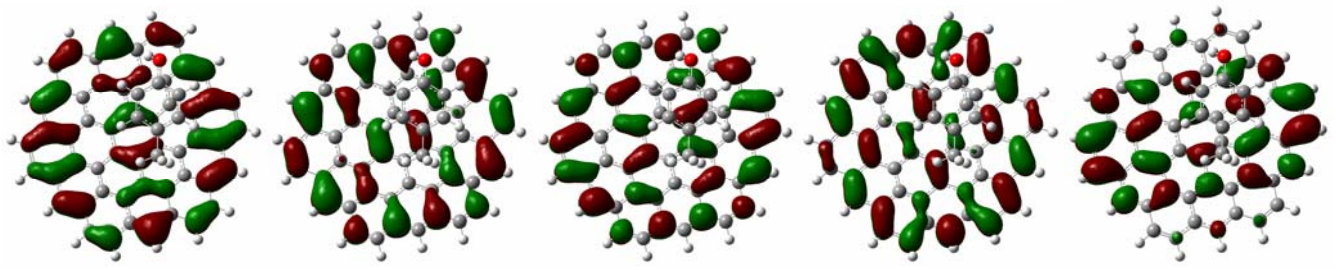

Y-GS^{2-} HDMO-2 HDMO-1 HDMO LUMO LUMO+1

Y-GS^{-} HDMO-1 HDMO SOMO LUMO LUMO+1

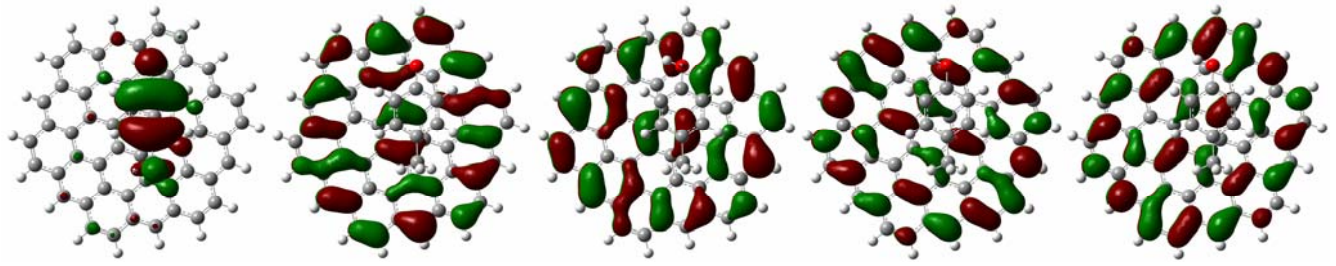

Y-GS^{0} HDMO-2 HDMO-1 HDMO LUMO LUMO+1

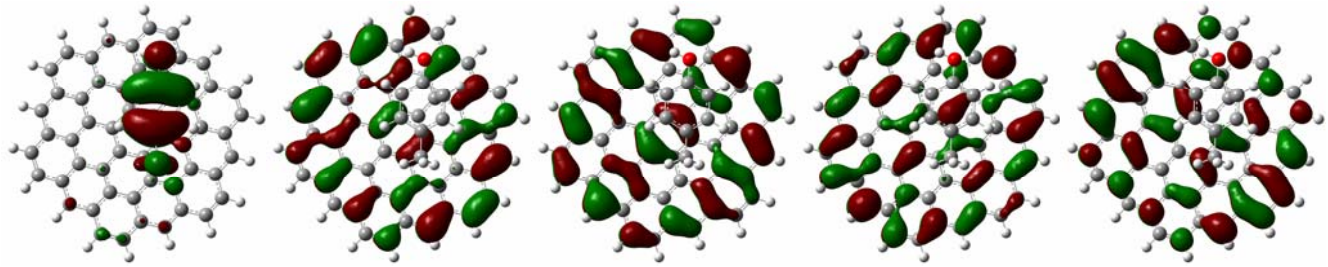

Y-GS^{+} HDMO-1 HDMO SOMO LUMO LUMO+1

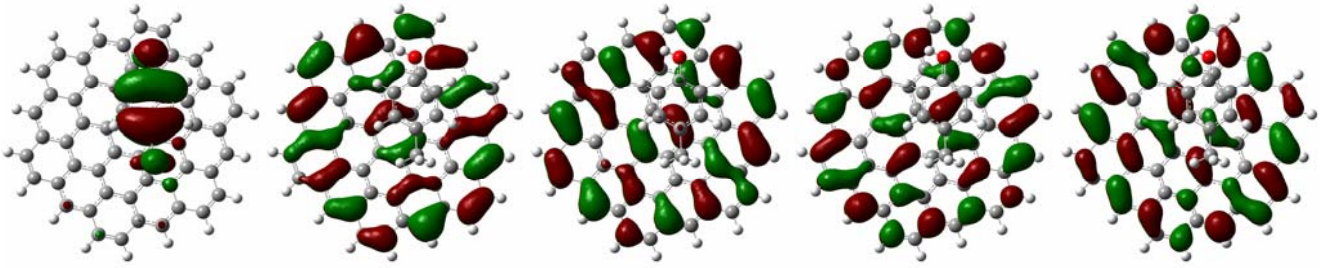

Y-GS^{2+} HDMO-1 HDMO LUMO LUMO+1 LUMO+2

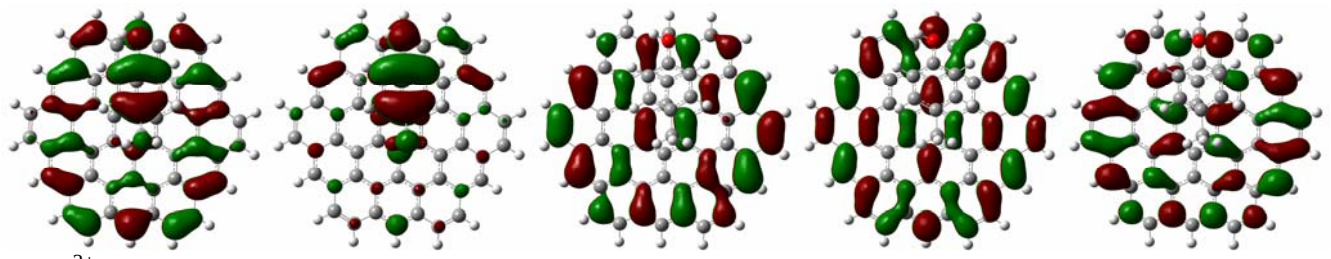

Y-GS^{3+} HDMO SOMO LUMO LUMO+1 LUMO+2

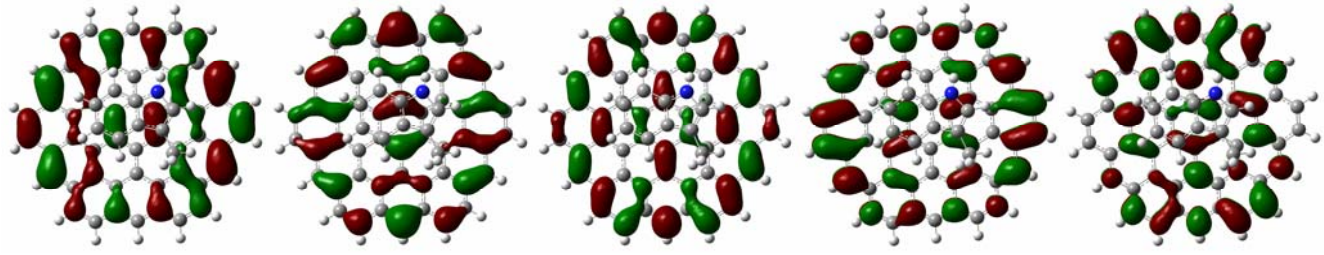

W-GS^{3-} HDMO-2 HDMO-1 HDMO SOMO LUMO

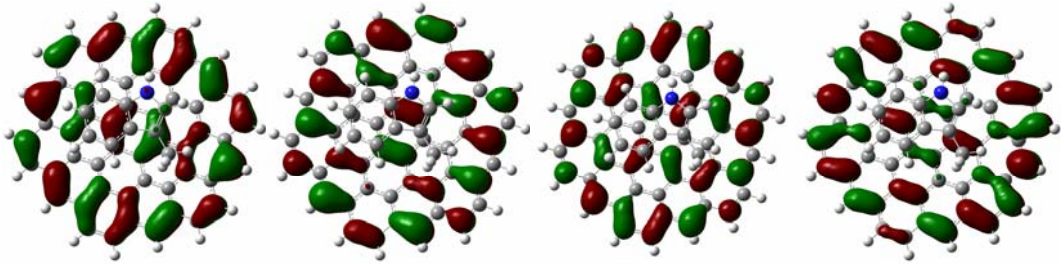

W-GS^{2-} HDMO-2 HDMO-1 HDMO LUMO LUMO+1

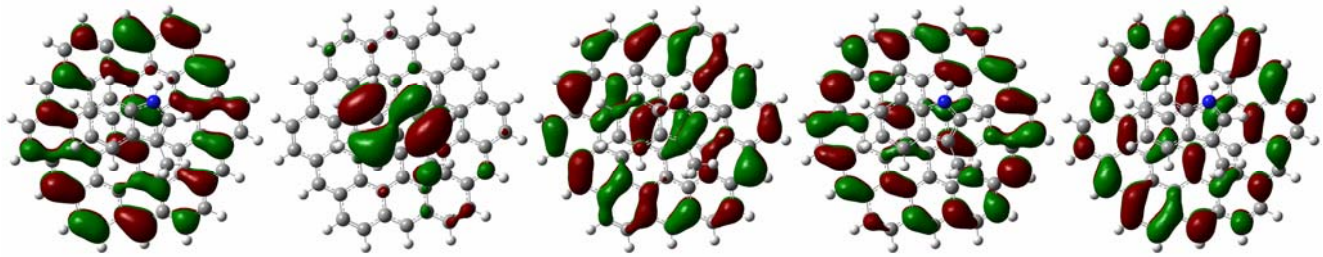

W-GS^{-} HDMO-1 HDMO SOMO LUMO LUMO+1

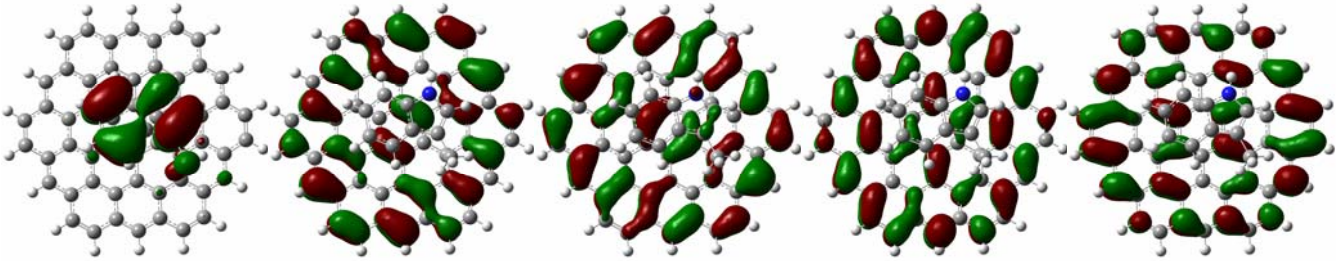

W-GS^{0} HDMO-2 HDMO-1 HDMO LUMO LUMO+1

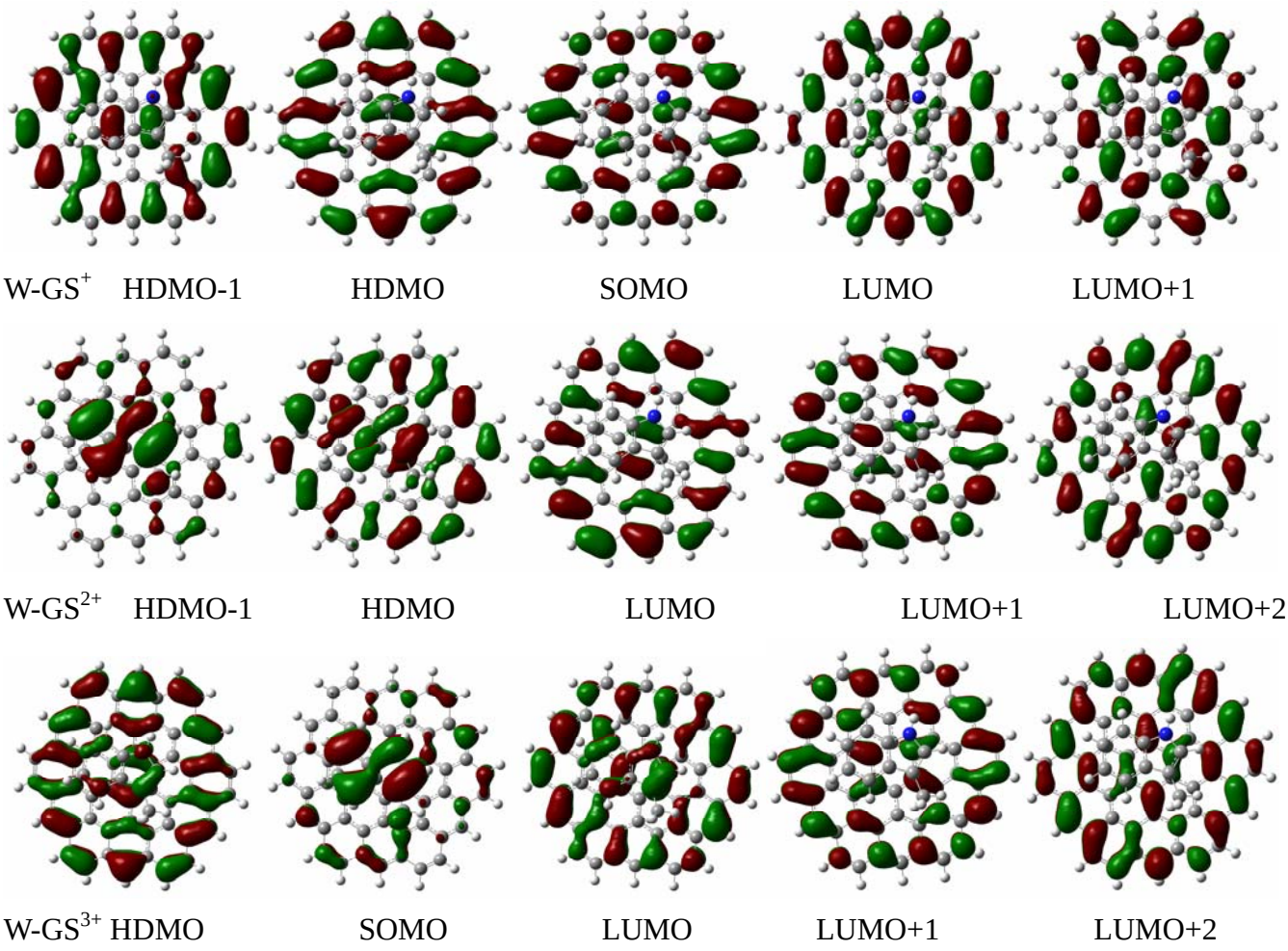

Figure S5. The distributions of the front molecular orbitals for the charged A-GS systems obtained by the M06-2X/6-31G(d) optimizations.

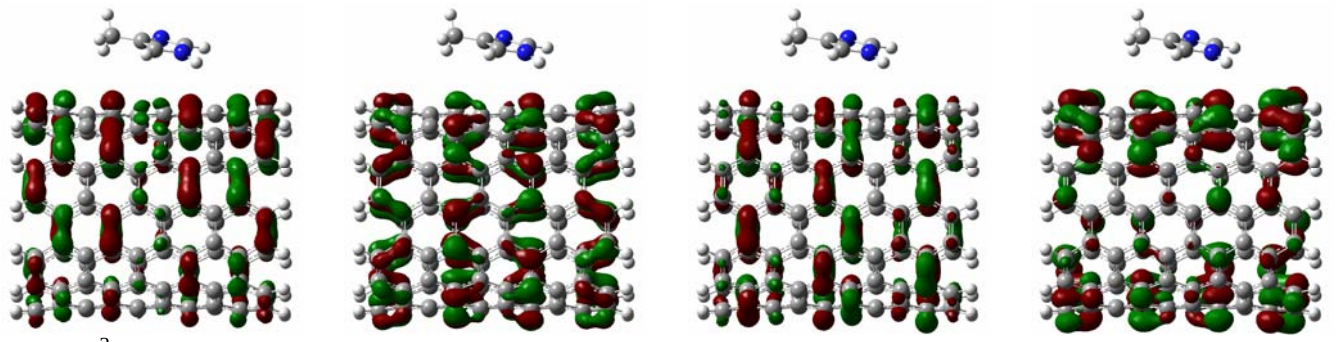

H-CNT^{3-} HDMO SOMO LUMO LUMO+1

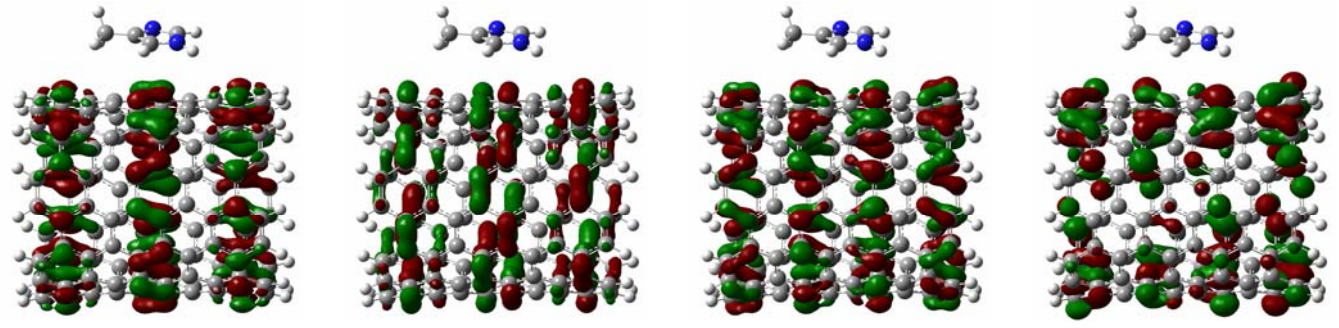

H-CNT^{2-} HDMO-1 HDMO LUMO LUMO+1

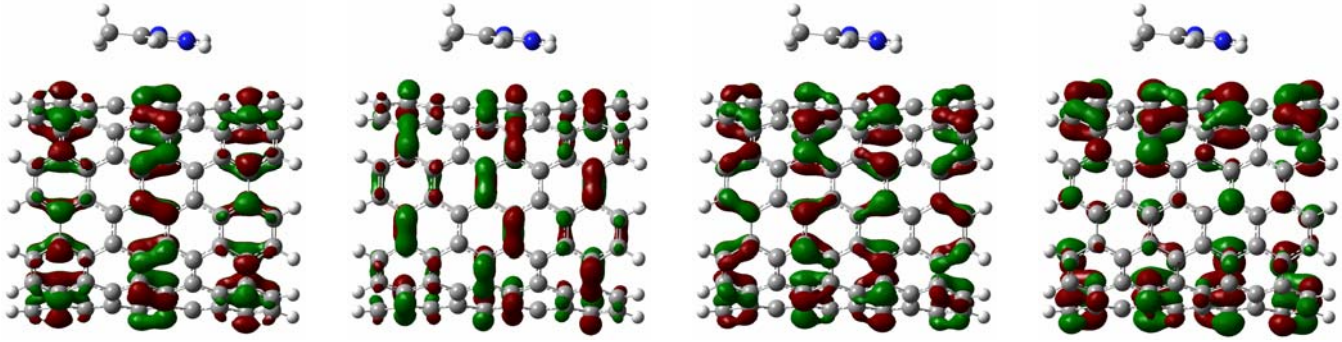

H-CNT^{-} HDMO SOMO LUMO LUMO+1

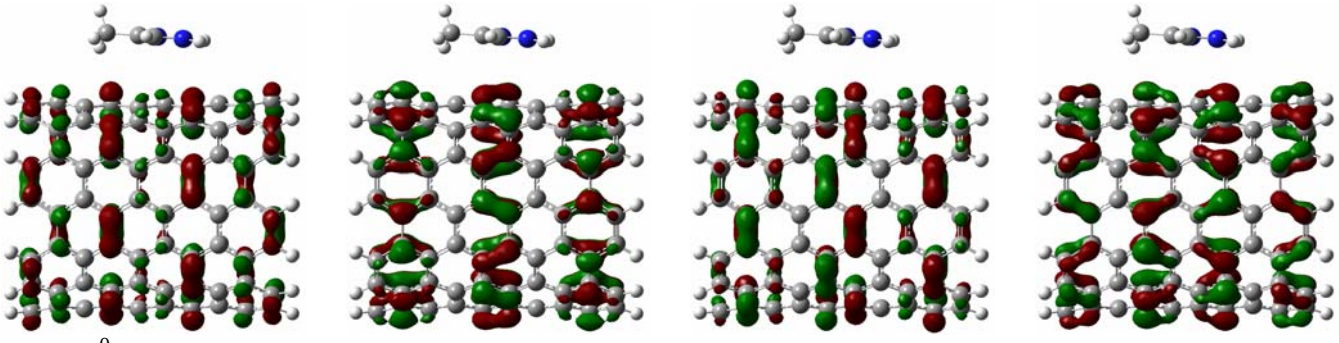

H-CNT^{0} HDMO-1 HDMO LUMO LUMO+1

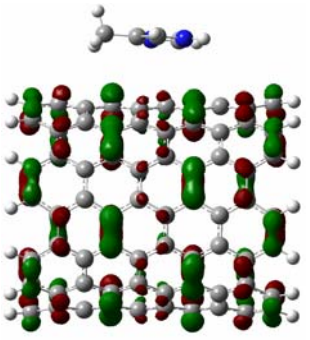

H-CNT^{+} HDMO

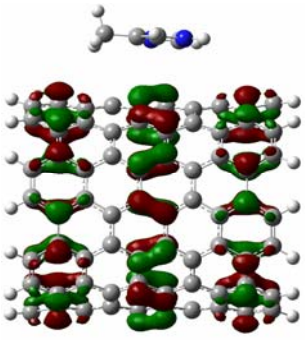

SOMO

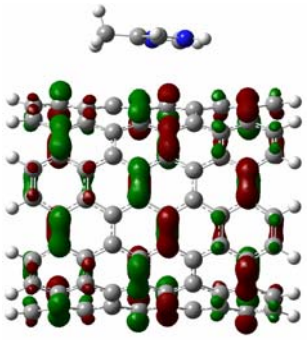

LUMO

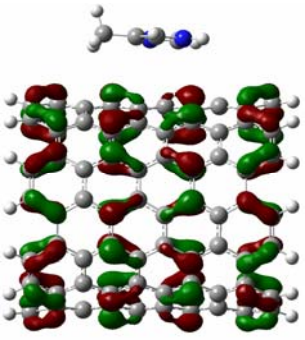

LUMO+1

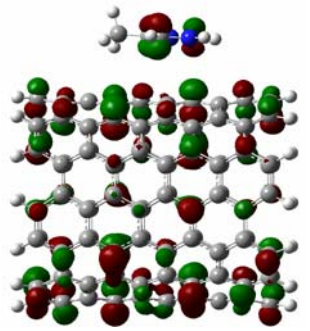

H-CNT^{2+} HDMO

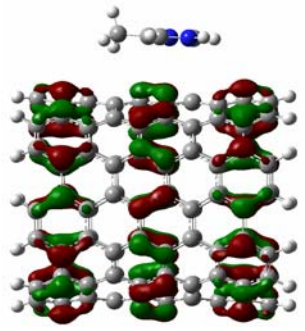

HDMO

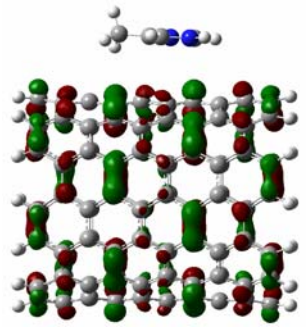

LUMO

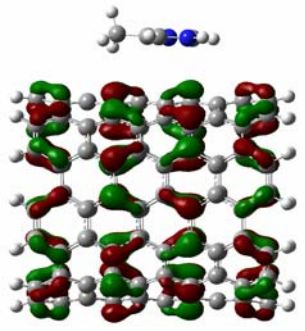

LUMO+1

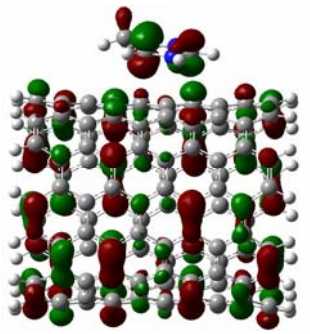

H-CNT^{3+} HDMO

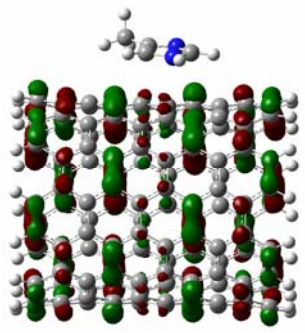

SOMO

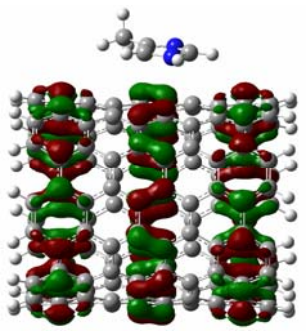

LUMO

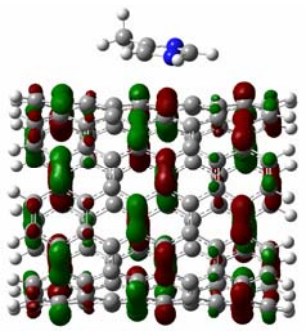

LUMO+1

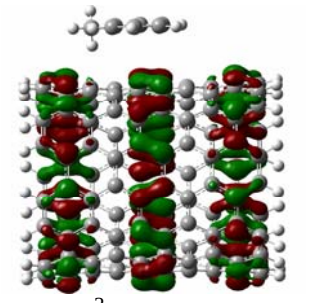

F-CNT^{3-} HDMO

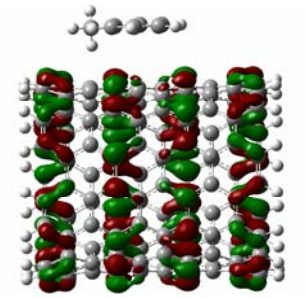

SOMO

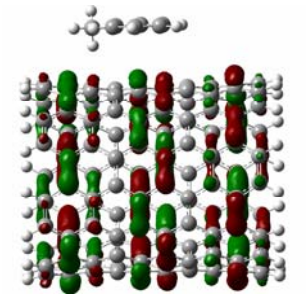

LUMO

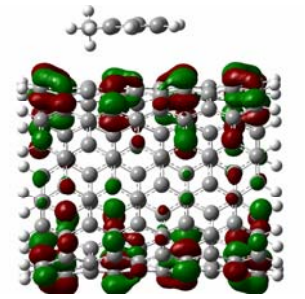

LUMO+1

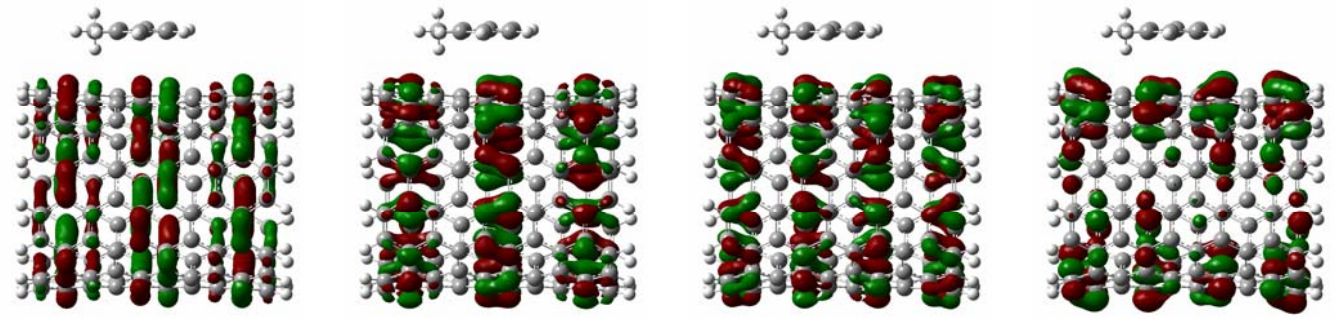

F-CNT^{2-} HDMO-1 HDMO LUMO LUMO+1

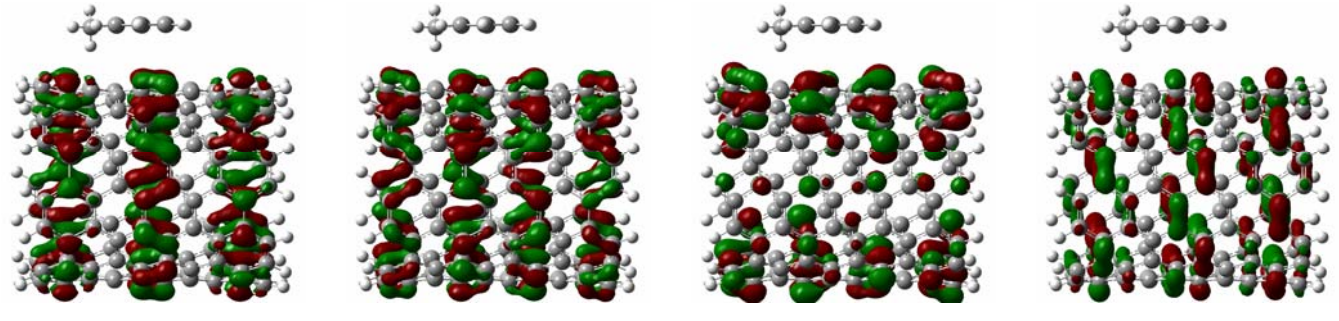

F-CNT^{-} HDMO SOMO LUMO LUMO+1

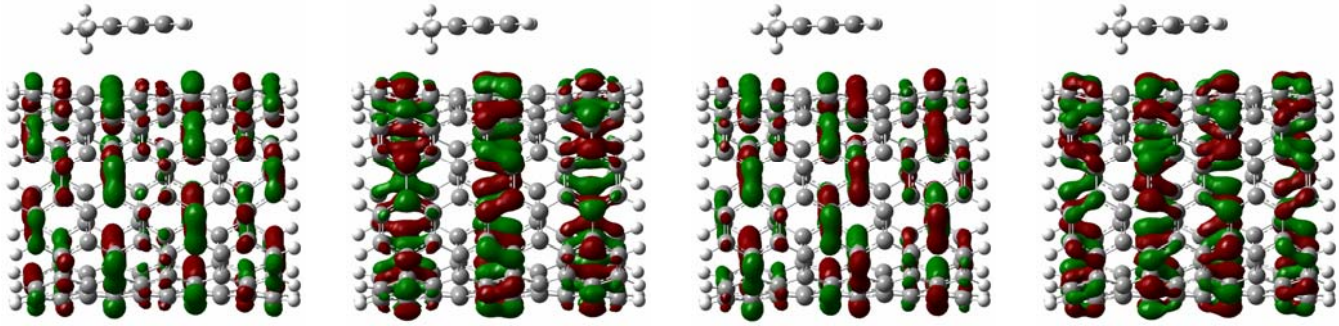

F-CNT^{0} HDMO-1 HDMO LUMO LUMO+1

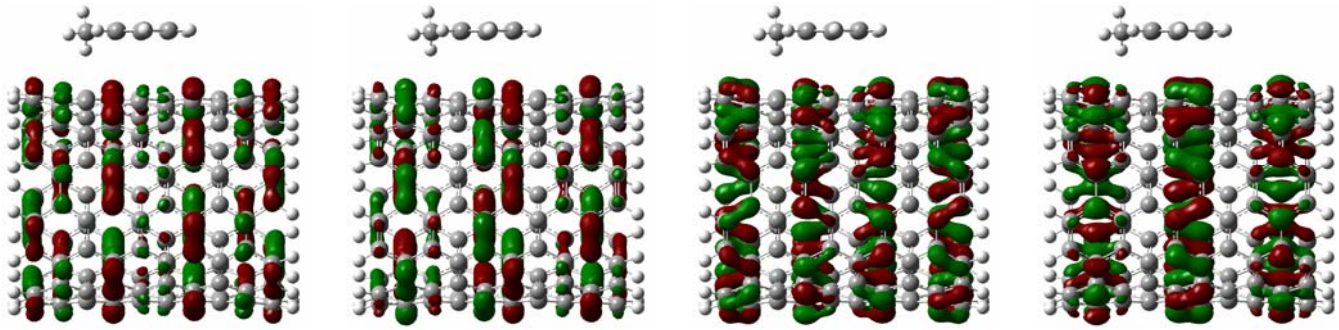

F-CNT^{+} HDMO SOMO LUMO LUMO+1

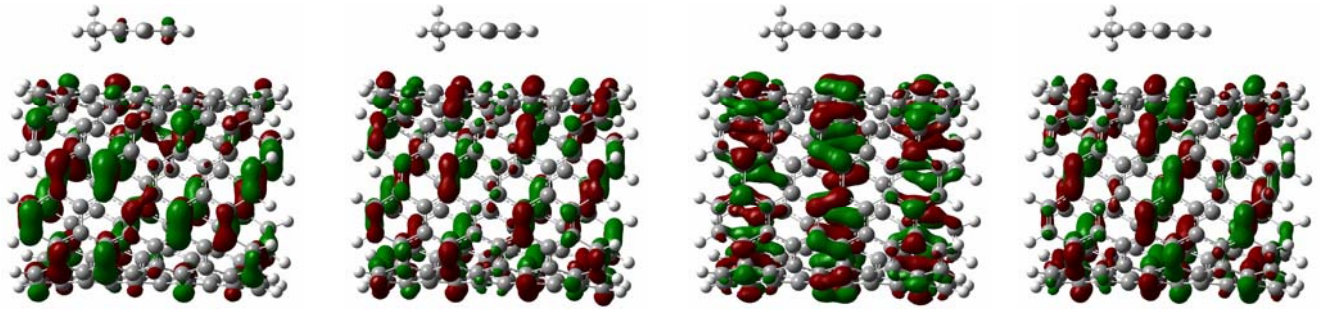

F-CNT^{2+} HDMO-1 HDMO LUMO LUMO+1

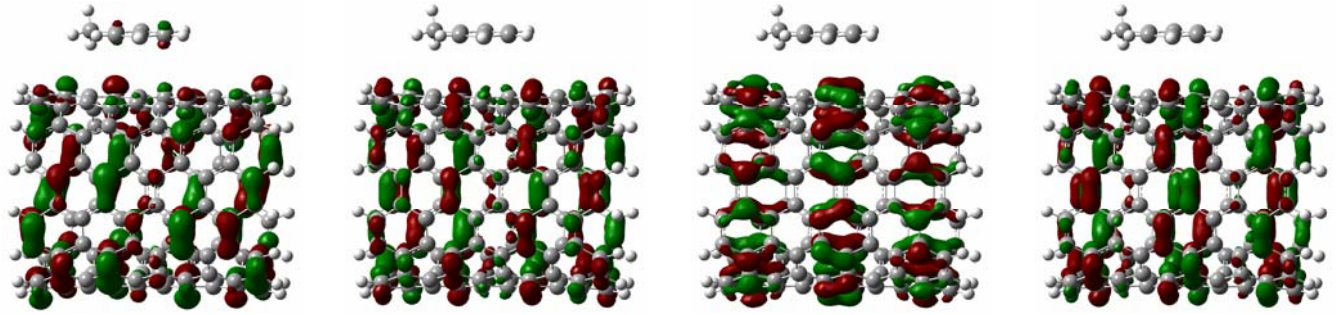

F-CNT^{3+} HDMO SOMO LUMO LUMO+1

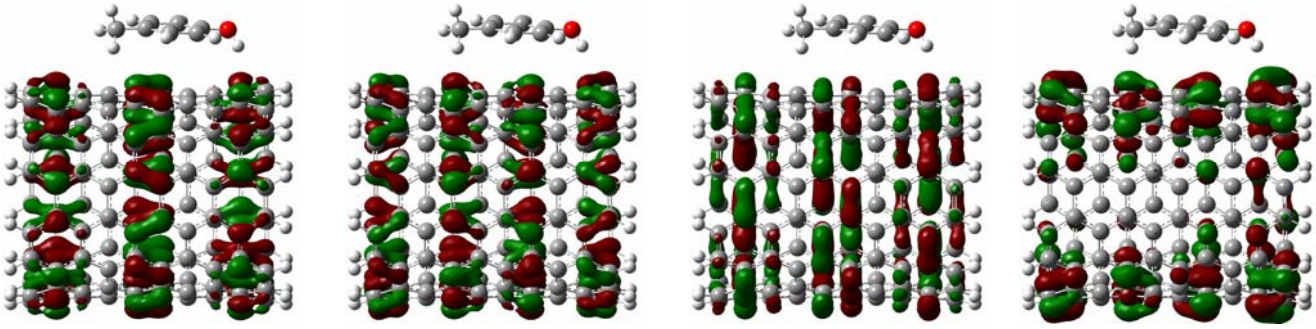

Y-CNT^{3-} HDMO SOMO LUMO LUMO+1

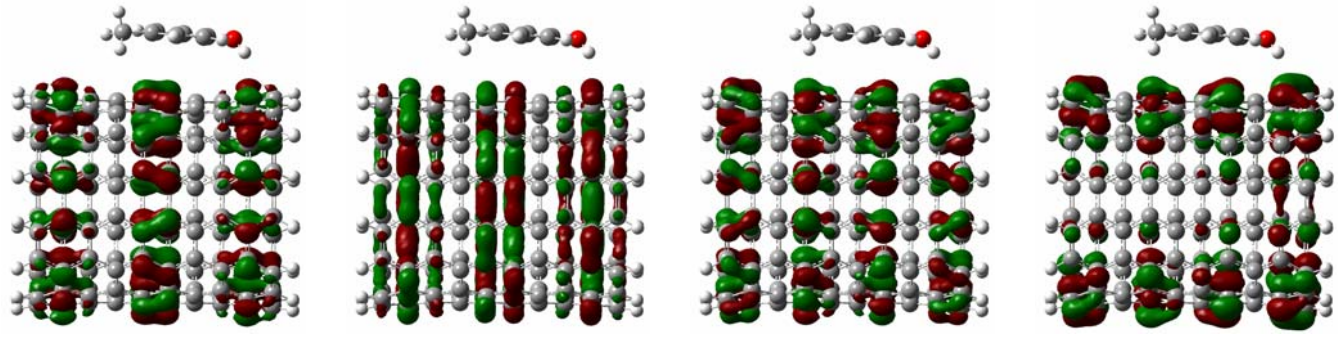

Y-CNT^{2-} HDMO-1 HDMO LUMO LUMO+1

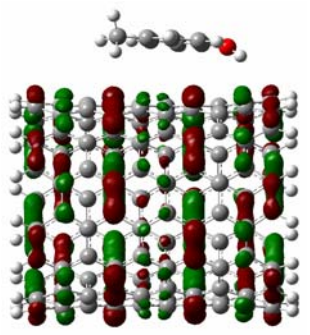

Y-CNT^{-} HDMO

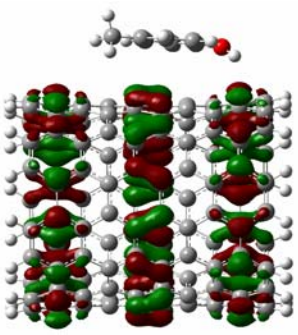

SOMO

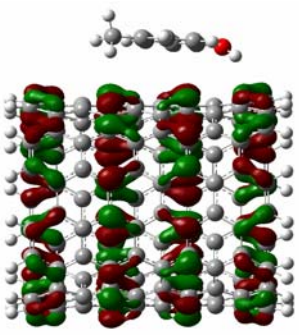

LUMO

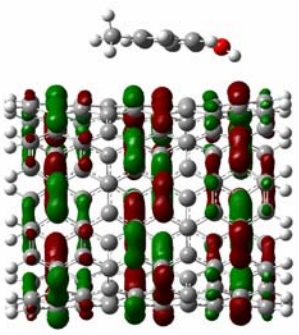

LUMO+1

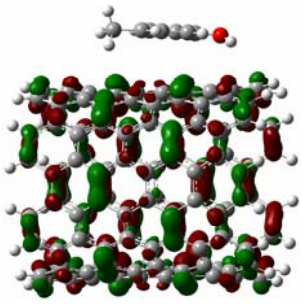

Y-CNT^{0} HDMO-1

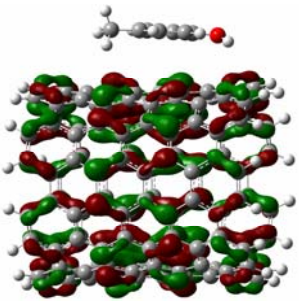

HDMO

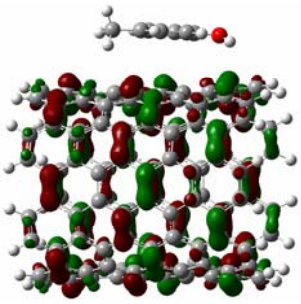

LUMO

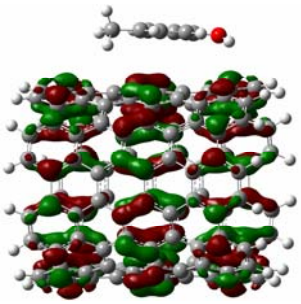

LUMO+1

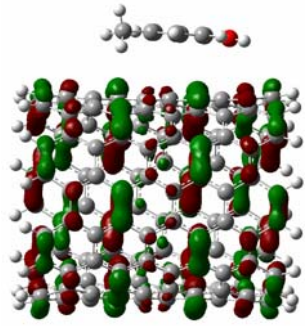

Y-CNT^{+} HDMO

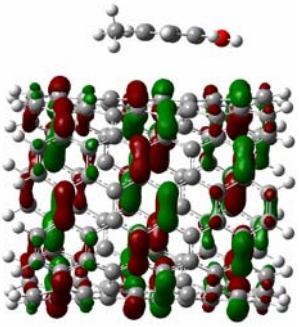

SOMO

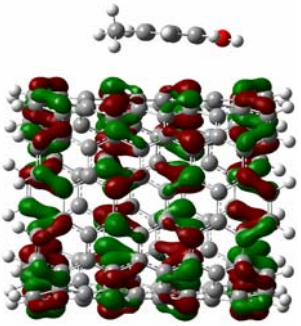

LUMO

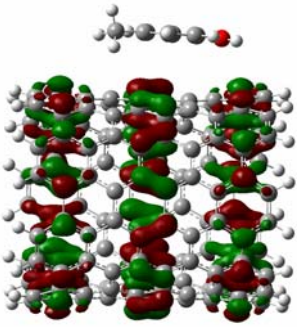

LUMO+1

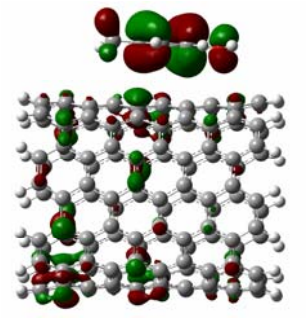

Y-CNT^{2+} HDMO-1

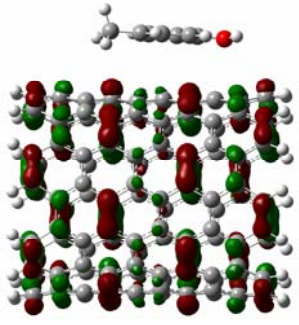

HDMO

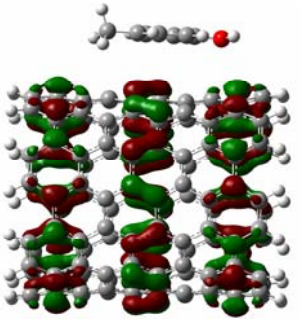

LUMO

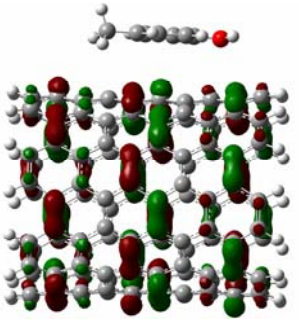

LUMO+1

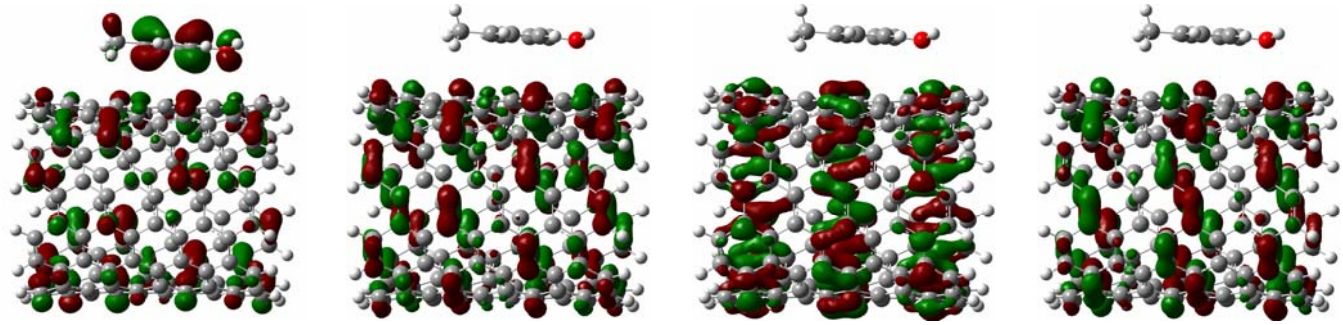

Y-CNT^{3+} HDMO SOMO LUMO LUMO+1

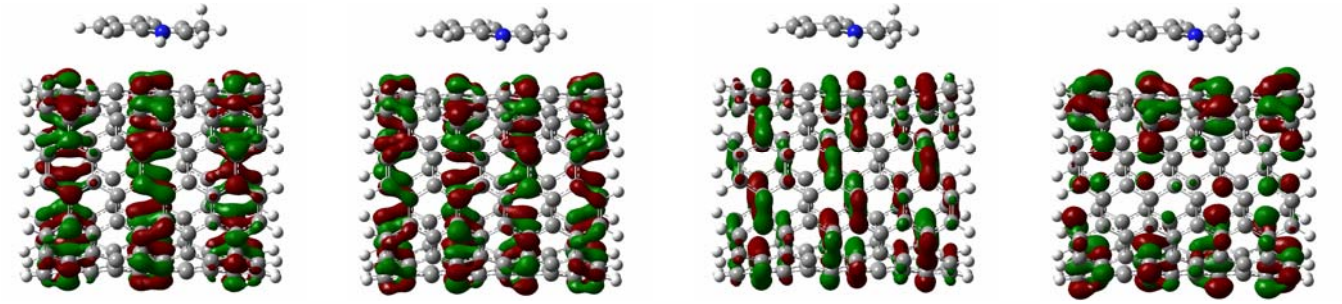

W-CNT^{3-} HDMO SOMO LUMO LUMO+1

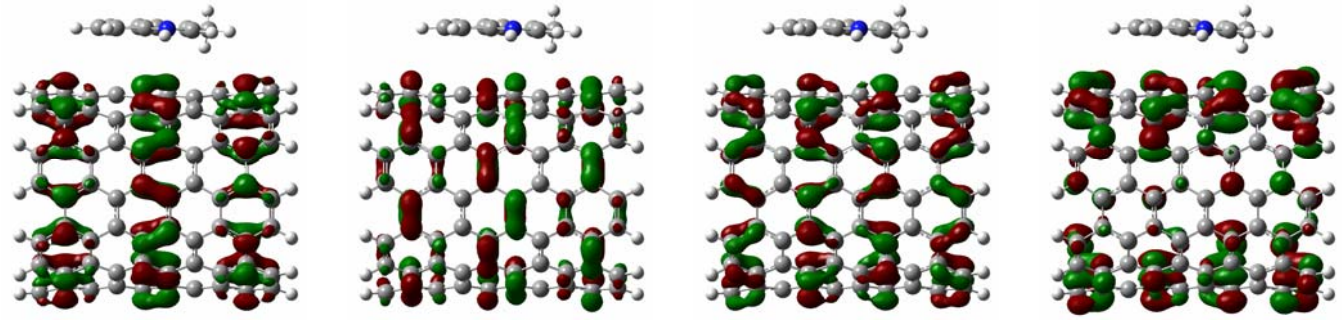

W-CNT^{2-} HDMO-1 HDMO LUMO LUMO+1

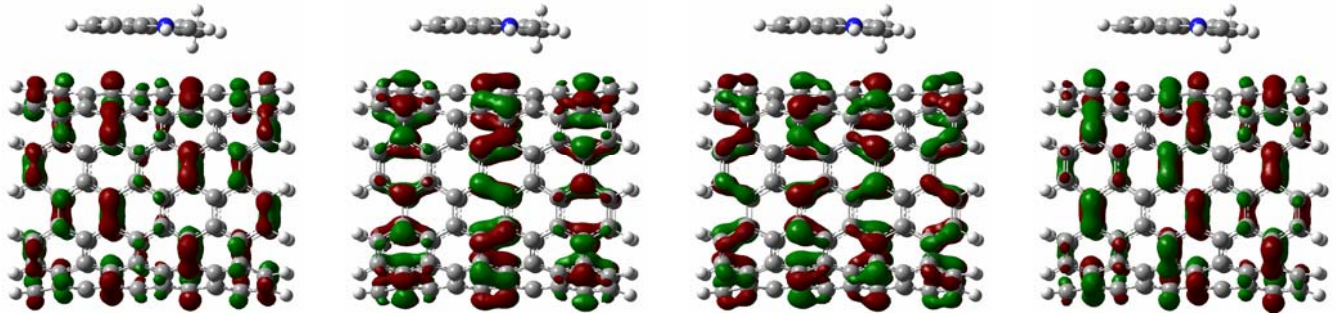

W-CNT^{-} HDMO SOMO LUMO LUMO+1

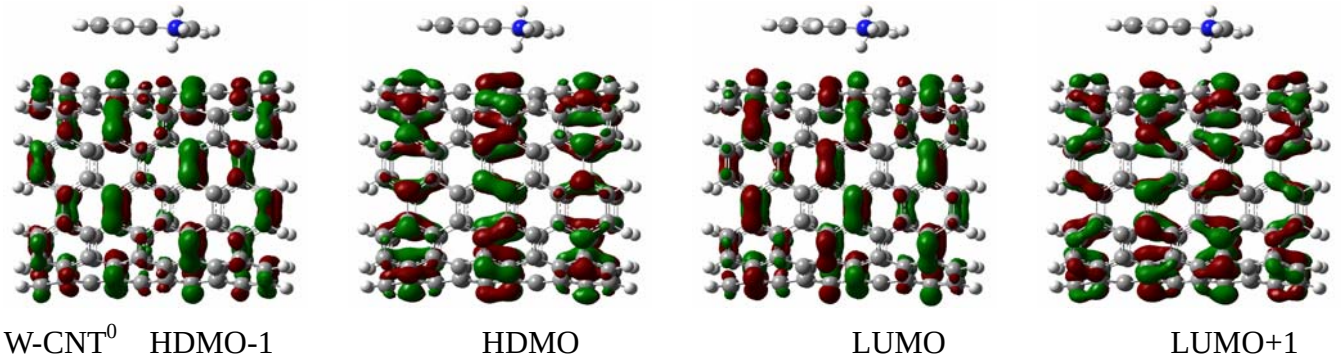

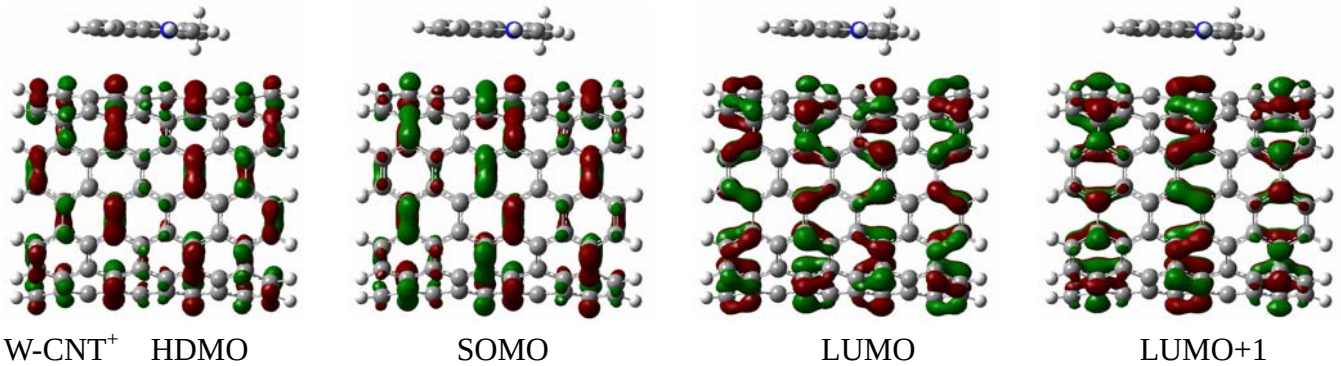

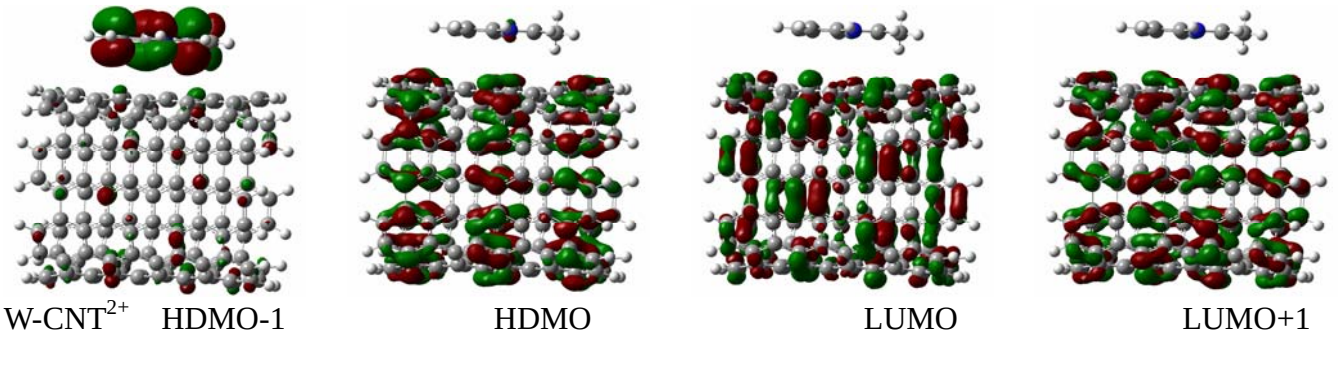

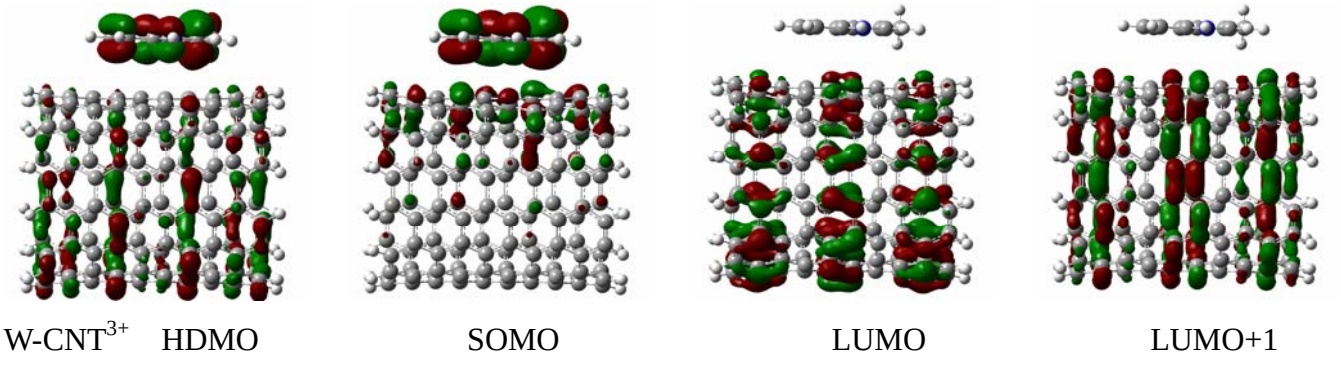

Figure S6 The distributions of the front molecular orbitals for the charged A-CNT systems by the M06-2X/6-31G(d) optimizations.

5. Electrostatic Potential

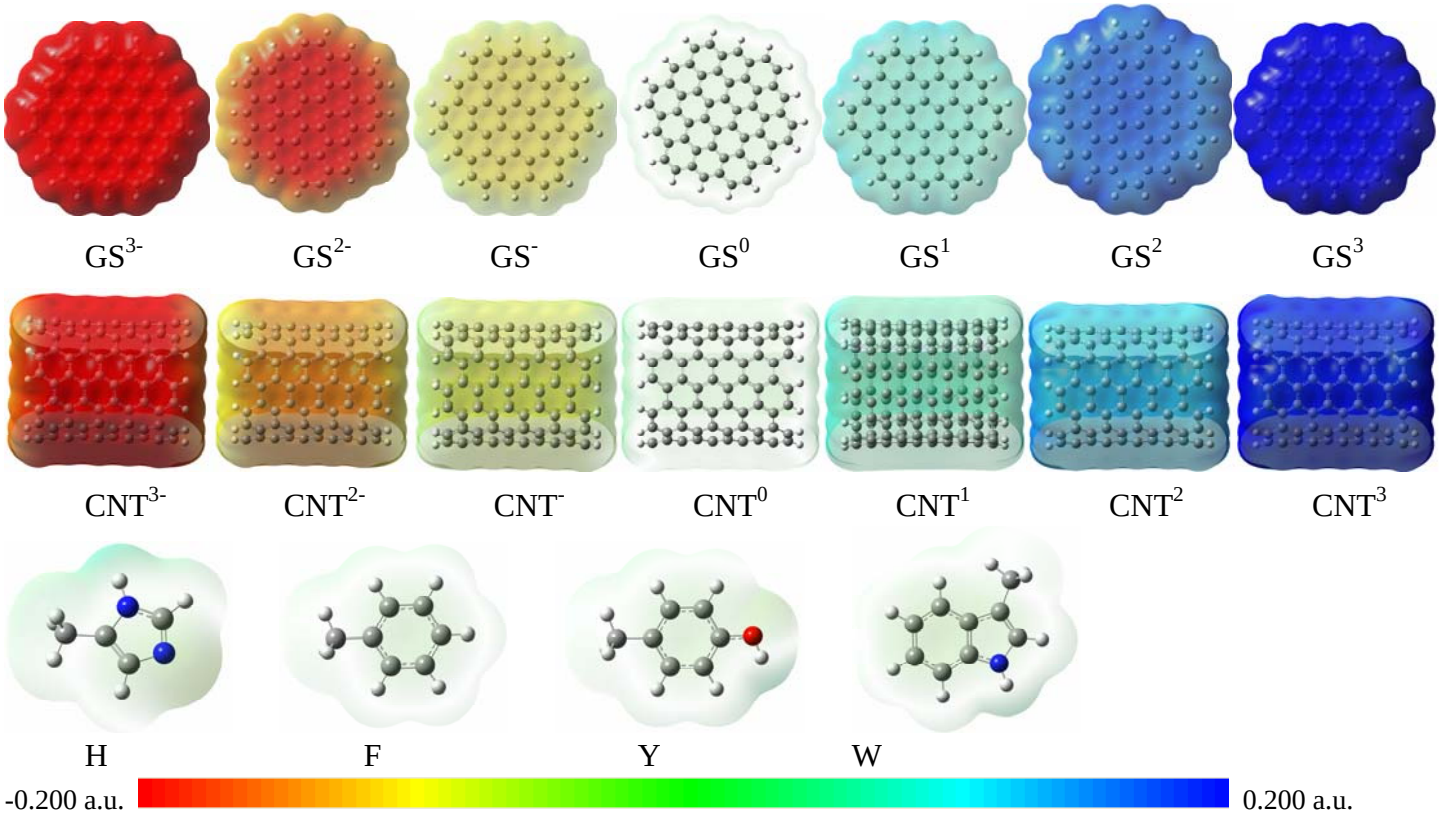

Figure S7. Electrostatic potential maps of GS^n, CNT^n(n=3-, 2-, 1-, 0, 1, 2, 3), H, F, Y and W. Electron-rich regions are shown in red and electron-poor regions are in blue.

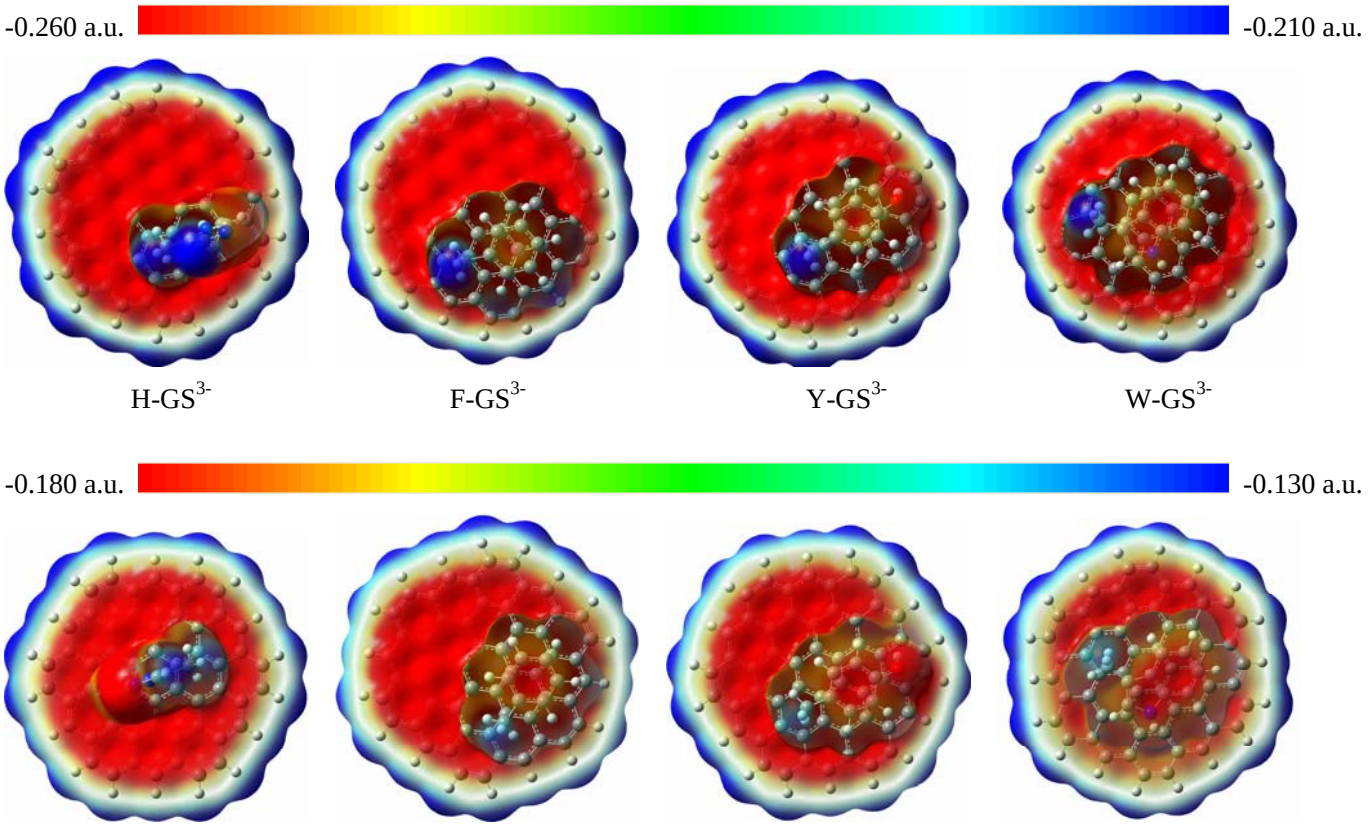

H-GS^{2-} F-GS^{2-} Y-GS^{2-} W-GS^{2-}

-0.060 a.u. -0.110 a.u.

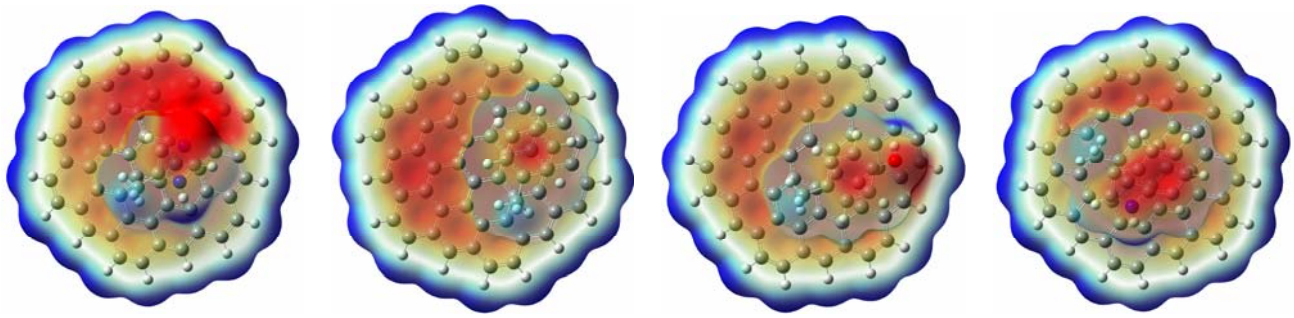

H-GS^{-} F-GS^{-} Y-GS^{-} W-GS^{-}

-0.025 a.u. 0.025 a.u.

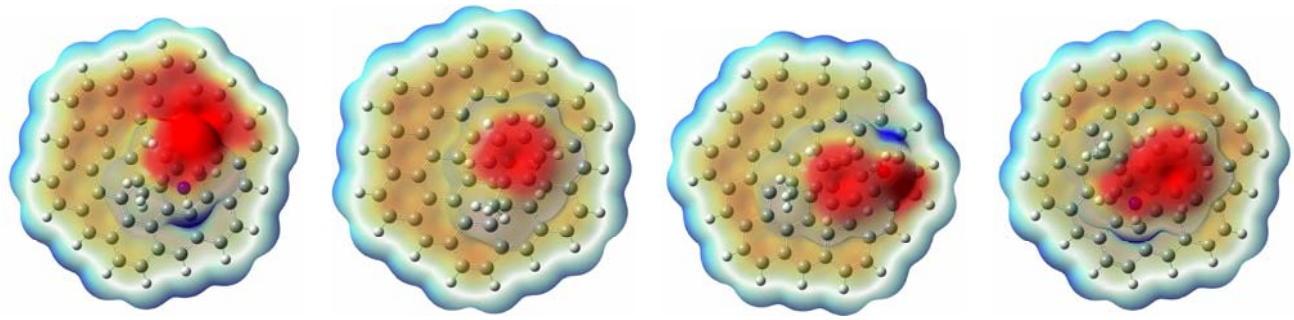

H-GS^{0} F-GS^{0} Y-GS^{0} W-GS^{0}

0.050 a.u. 0.100 a.u.

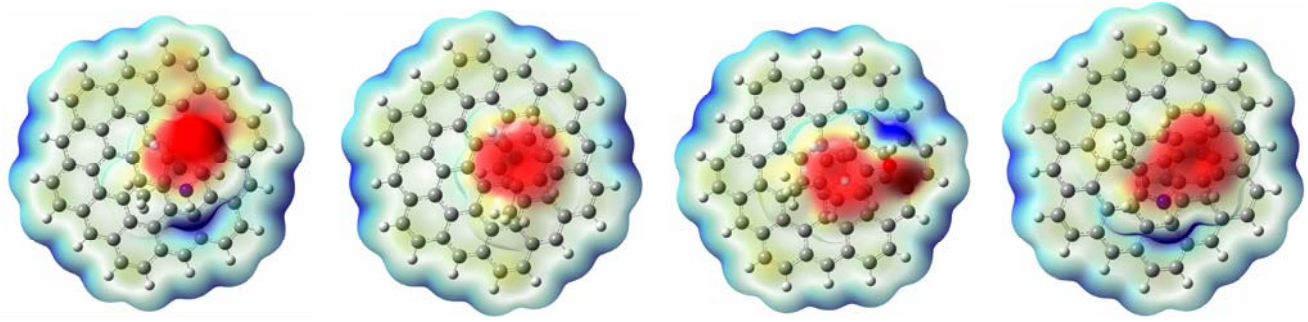

H-GS^{+} F-GS^{+} Y-GS^{+} W-GS^{+}

0.120 a.u. 0.170 a.u.

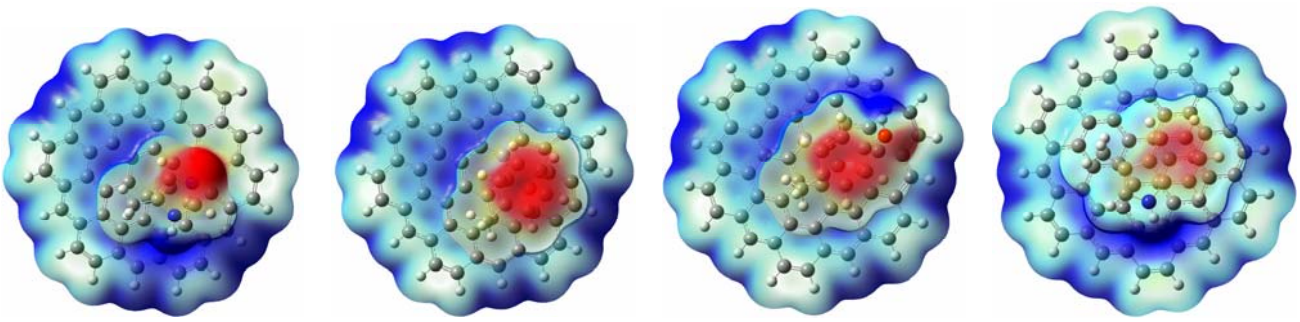

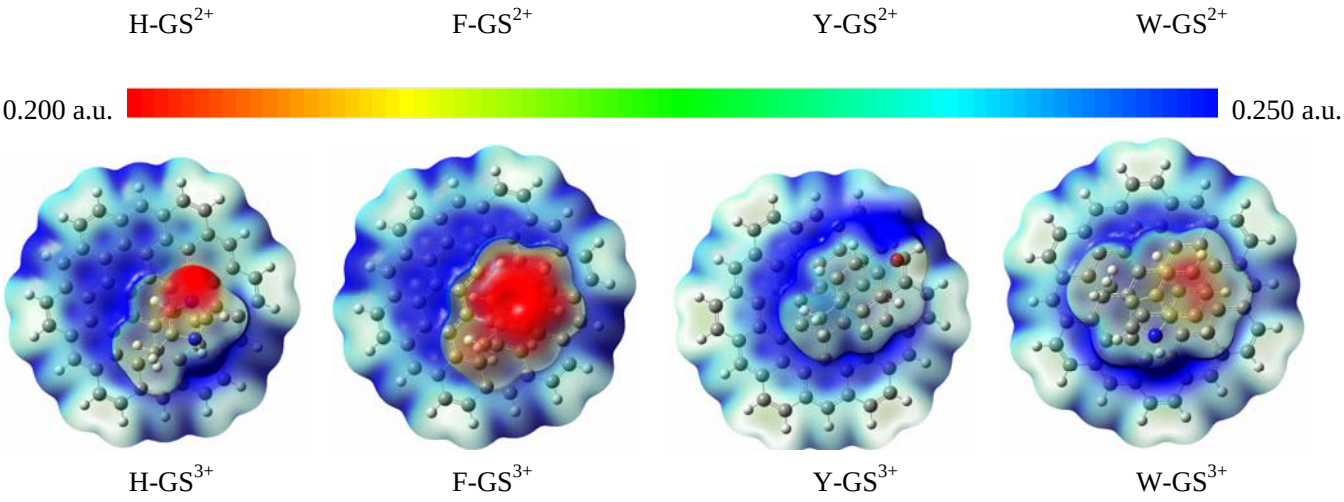

Figure S8. Electrostatic potential maps of A-GS^{n}(n=3-, 2-, 1-, 0, 1, 2, 3) showing the charge distributions throughout the inclusion complexes. To highlight the different charge regions, the criterions of the electron density surfaces are different for the different charged states. Regions of high electron density are red and electron poor regions are blue. It is clear that the charges mainly delocalize over the GS for all the A-GS^{n} (n= 3-, 2-, 1-, 1, 2, 3) systems except for W-GS^{3+} and Y-GS^{3+}.

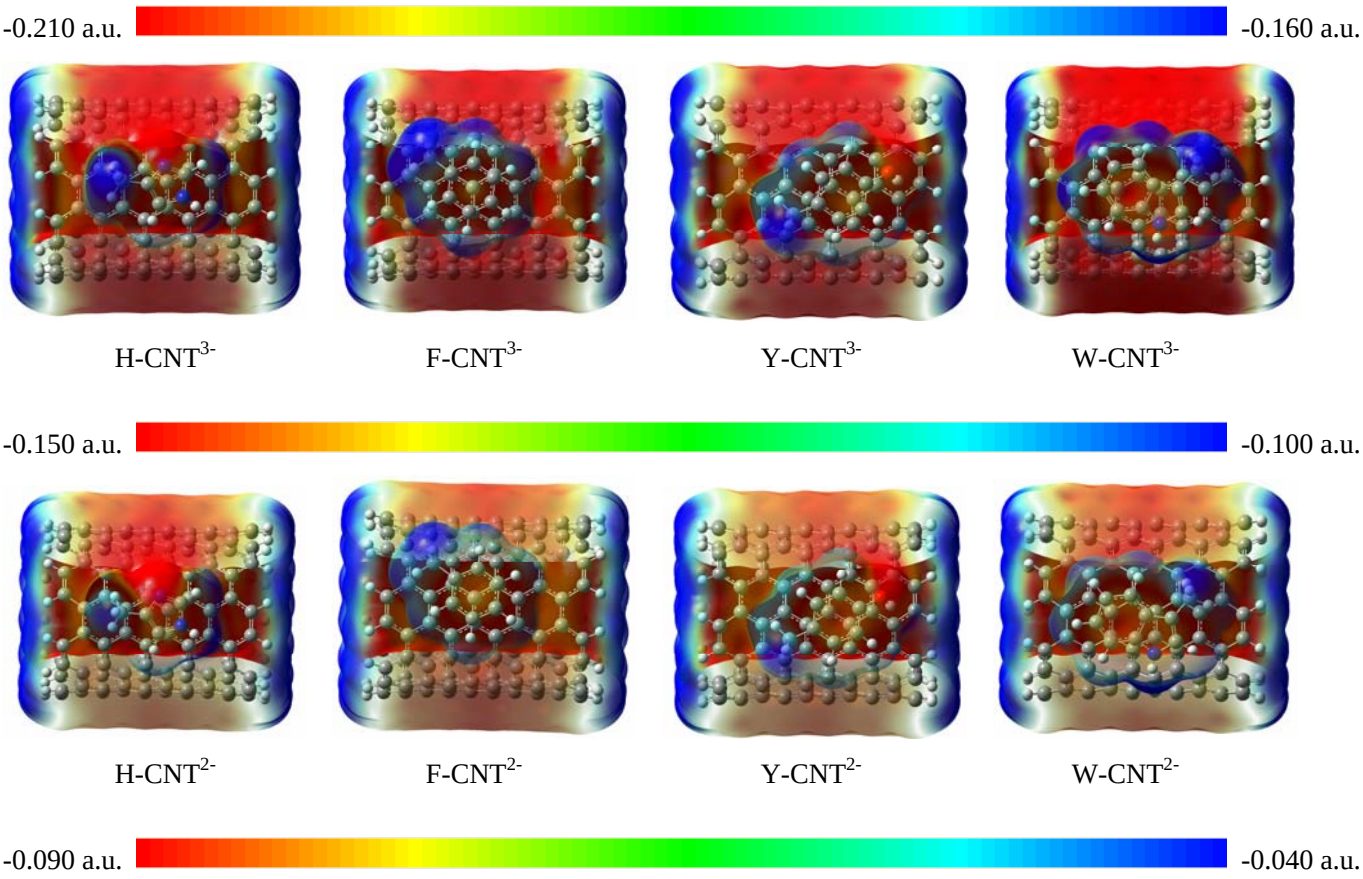

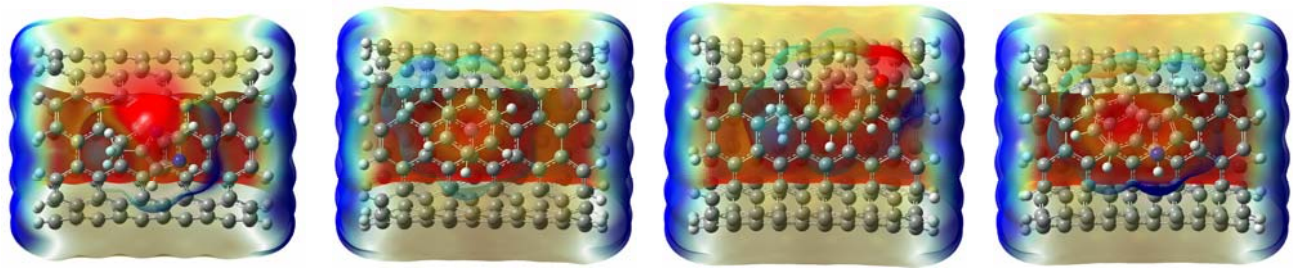

H-CNT^{-} F-CNT^{-} Y-CNT^{-} W-CNT^{-}

-0.025 a.u. 0.025 a.u.

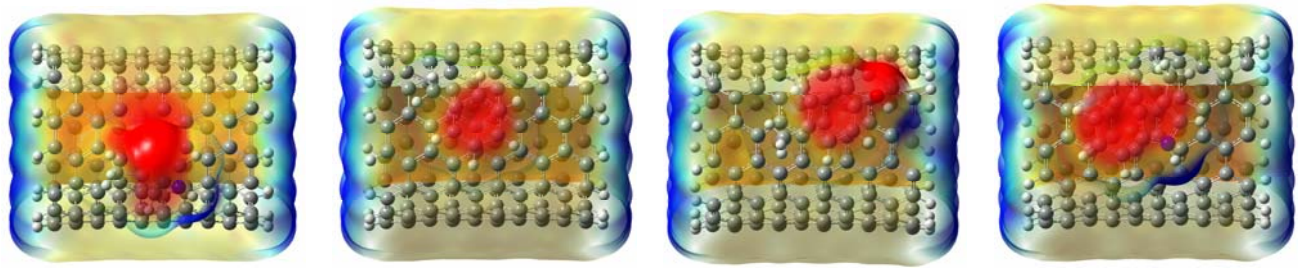

H-CNT^{0} F-CNT^{0} Y-CNT^{0} W-CNT^{0}

0.020 a.u. 0.070 a.u.

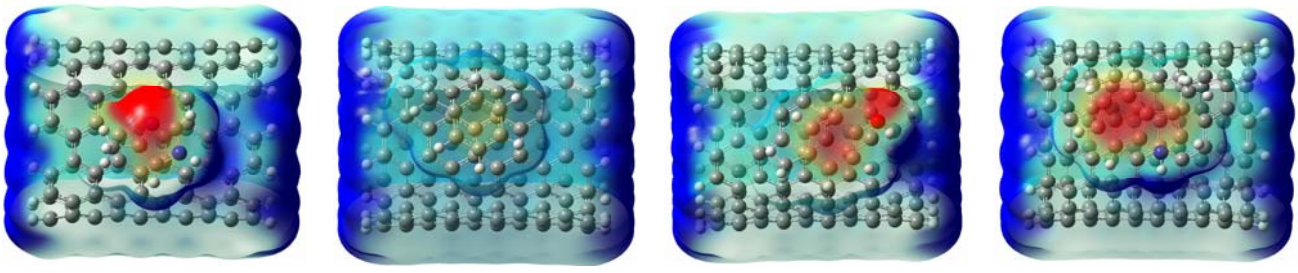

H-CNT^{+} F-CNT^{+} Y-CNT^{+} W-CNT^{+}

0.080 a.u. 0.130 a.u.

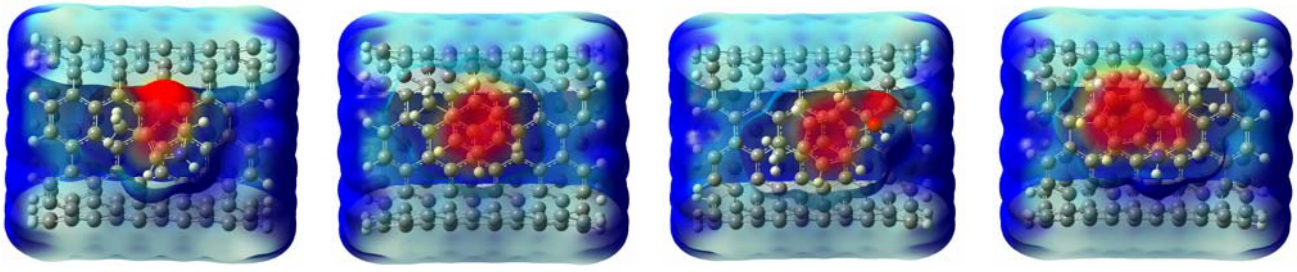

H-CNT^{2+} F-CNT^{2+} Y-CNT^{2+} W-CNT^{2+}

0.150 a.u. 0.200 a.u.

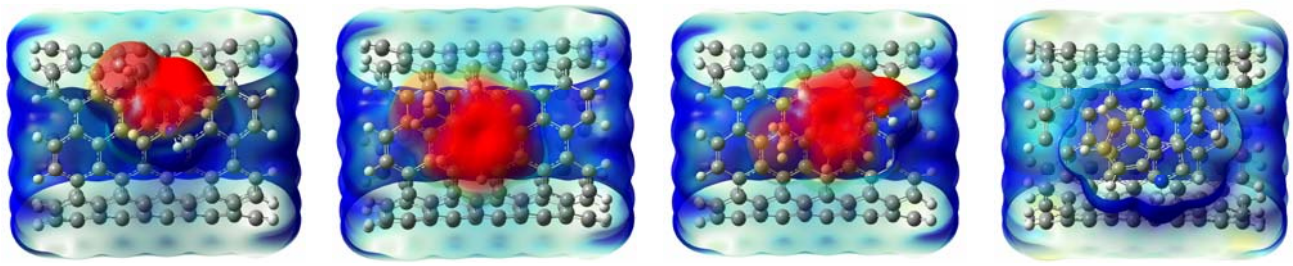

H-CNT^{3+} F-CNT^{3+} Y-CNT^{3+} W-CNT^{3+}

Figure S9. Electrostatic potential maps of A-CNT^{n} (n=3-, 2-, 1-, 0, 1, 2, 3) showing the charge distributions throughout the inclusion complexes. To highlight the different charge regions, the criterions of the electron density surfaces are different for the different charged states. Regions of high electron density are color coded red and electron poor regions are blue. It is clear that the charges mainly delocalize over the CNT for all the A-CNT^{n} (n= 3-, 2-, 1-, 1, 2, 3) systems except for W-CNT^{3+}.

Note: Figure S7 clearly displays that the negative molecular electrostatic potential (red color) occurs in the more negative charged GS and CNT and the positive molecular electrostatic potential (blue color) increases with the increase of the system positive charges. The isovalues of electrostatic potential surfaces of H, F, Y and W are in line with that of neutral GS or CNT (Figure S7). Figure S8 and S9 show that the charges mainly delocalize over the GS and CNT. Therefore, the increasing charges of GS (or CNT) can enhance the electrostatic interactions between the surface of GS (or CNT) and the aromatic rings. Because the charges are delocalized over the GS and CNT, the charge isodensity of CNT^{n} is lower than that of the same charged GS^{n}, as shown in Figure S7. Therefore, the electrostatic interaction between CNT and aromatic ring in A-CNT^{n} is lower than that in A-GS^{n}.